Spatio-temporal evaluation of entropy-based source localization in magnetoencephalography

Tanguy Hedrich

Master of Engineering

Biomedical Engineering Department

McGill University

3775, rue University, room 316. Montréal, QC H3A 2B4 Canada

2013-12-13

A thesis submitted in partial fulfillment of the requirements for the degree of Master of Engineering

ACKNOWLEDGEMENTS

I would like to express my very great appreciation to Dr Christophe Grova, my supervisor, for his patient guidance, enthusiastic encouragement and useful critique of this research work.

I am particularly grateful for the assistance given by Dr Jean-Marc Lina. His willingness to give his time so generously has been very much appreciated.

My grateful thanks are also extended towards Dr. Eliane Kobayashi and Dr. Marcel Heers for sharing their clinical knowledge to help me with this project.

I would also like to thank my colleagues and friends Ms. Rasheda Chowdhury, Ms. Kangjoo Lee, and Mr. Alexis Machado, for their help, their advice and their moral support, which helps me to work in the best conditions.

I wish to thank my parents for their tremendous contributions and support both morally and financially towards the completion of this project.

Finally I also show my gratitude to my friends and all who contributed in one way or the other during the course of the project.

ABSTRACT

For 30% of patients affected by focal epilepsy, a surgical intervention is considered to remove the zone of the brain triggering the seizures. Interictal spikes are transient epileptic discharges, occurring between seizures. During presurgical investigation of patients affected by focal epilepsy, magnetoencephalography (MEG) source localization is used to detect the brain region where interictal spikes occur.

The estimation of the size of the brain region generating the epileptic discharge may be a useful piece of information for the estimation of the resection area. Moreover, the interictal spike may propagate along the cortical surface. It is crucial during presurgical investigation to detect propagation pattern to identify the onset of the epileptic discharges.

Maximum entropy on the mean (MEM) is a source localization method which allows one to introduce a reference distribution containing prior information about MEG data. This reference distribution is based on the assumption that the brain is divided into parcels of generators that can be considered as active or not. It has already been demonstrated that this method is sensitive to the spatial extent of the source. Coherent MEM (cMEM) is a version of MEM adding a spatial smoothness constraint within the parcels. In this thesis, MEM and cMEM were compared to a standard source localization technique: the minimum norm estimate (MNE).

The first objective of the thesis was to test the performance to estimate the time course of a simulated epileptic spike. We simulated interictal spikes propagating along the cortical surface. Real MEG background data were used to corrupt noise-free simulations, thus providing realistic simulated data. We demonstrated that MEM and cMEM provided excellent spatial detection scores and a similar temporal accuracy to MNE.

We then evaluated the spatial accuracy of the source localization methods using the resolution matrix, which can be seen as the set of all the point spread functions of the source localization methods. MEM and cMEM resolution matrices were estimated using Monte Carlo simulations. The results showed that MEM and cMEM have higher theoretical spatial resolution than MNE.

Finally, a method was proposed to obtain a map of activation based on a non parametric statistical analysis. The map was performed using a bootstrap-based analysis in the time-frequency domain. We found that the results varied with the spatial extent of the source. However, the variance of the estimate of the null distribution seemed to be underestimated as the statistical map lacked specificity.

ABRÉGÉ

Pour 30% des patients touchés par une épilepsie focale, une intervention chirurgicale peut être envisagée en vue de réséquer la zone du cerveau provoquant les crises d'épilepsie. Les pointes intérictales sont des évennements épileptiques transitoires, se produisant entre les crises d'épilepsie. Pendant la prise en charge préchirurgicale de ces patients, la localisation de source en magnétoencéphalographie (MEG) est utilisée pour détecter la région du cerveau où les pointes intérictales se produisent.

L'estimation de la taille des décharges épileptiques peut être une information utile pour l'estimation de la zone à réséquer. De plus, une pointe épileptique peut se propager le long de la surface corticale. Il est crucial pendant l'exploration préchirurgicale de localiser un tel circuit de propagation pour s'assurer d'identifier la zone initiale des décharges épileptiques.

Le maximum d'entropie sur la moyenne (MEM) est une technique de localisation de source qui permet d'introduire une distribution de référence contenant des informations a priori sur les données MEG. Cette distribution de référence est basée sur l'hypothèse que le cerveau est divisé en parcelles de générateurs qui peuvent être considérées comme actives ou non. Il a déjà été prouvé que cette méthode était sensible à l'extention spatiale de la source. Le MEM cohérent (*coherent MEM* - cMEM) est une version du MEM qui ajoute une contrainte de lissage spatial à l'intérieur des parcelles. Pour ce mémoire, MEM et cMEM ont été comparés à

une technique de localisation de source standard : l'estimation de norme minimale (*minimum norm estimate* - MNE)

Le premier objectif de ce mémoire est de tester la performance de l'estimation du décours temporel d'une pointe. Nous avons généré des simulations de pointes intericales se propageant le long de la surface corticale, entachées par du bruit de fond réaliste. Nous avons montré que MEM et cMEM obtenaient d'excellents scores de détection spatiale, ainsi qu'une précision temporelle similaire au MNE.

Ensuite, nous avons évalué la précision spatiale des méthodes de localisation de source en utilisant la matrice de résolution, qui peut être vue comme l'ensemble de toutes les fonctions d'étalement de point des méthodes de localisation de sources. Les matrices de résolution du MEM et du cMEM ont été estimées en utilisant des simulations de Monte Carlo. Les résultats ont montré que MEM et cMEM avaient une meilleure résolution spatiale théorique que MNE.

Finalement, nous avons proposé une méthode visant à obtenir une carte d'activation se basant sur une analyse statistique non paramétrique. La réalisation de la carte statistique s'est faite avec une méthode utilisant le rééchantillonnage bootstrap dans le domaine temps-échelle. Nous avons trouvé que les résultats variaient avec l'extention spatiale de la source estimée. Cependant, la variance de l'estimation de la distribution de l'hypothèse nulle semblait être sous-estimée, étant donné que la carte statistique manquait de spécificité.

TABLE OF CONTENTS

LIST OF TABLES

LIST OF FIGURES

Chapter 1
Introduction

Epilepsy affects 1% of the population in Canada [91]. About two third of the patients have their symptoms controlled by long-term drug therapy. The other third is resistant to treatment with anti-epileptic medication. Among them, the patients with focal epilepsy (i.e. where the seizures are triggered by a limited brain region) are potential candidates for epilepsy surgery. The part to be resected is determined after a thorough presurgical investigation, which includes, besides clinical exam and seizure semiology [1] , electrophysiology and neuroimaging studies as well as neuropsychological evaluations.

Epileptic events are mainly due to an excessive and sudden activation of pyramidal cells, a type of neuron located on the cortical surface and in the hippocampus and the amygdala. Interictal spikes consist of rapid neuronal discharges (lasting a few hundred milliseconds) that are not associated with any clinical manifestation; the patient is unaware of having them. One can record and detect these spontaneous abnormal discharges from scalp electroencephalography (EEG) or magnetoencephalography (MEG) only when a spatially extended portion of the cortex is involved during the generation of the discharge. Scalp EEG is

1. Semiology is the study of signs and symptoms.

a standard exploration technique using electrodes on the surface of the head to record neuronal bioelectrical activity, whereas MEG detects the corresponding magnetic fields. Both modalities are used in the presurgical evaluation to localize the source of the interictal spike: the so-called irritative zone. In this thesis, MEG was considered because of its higher spatial accuracy. Indeed, magnetic fields are not distorted by the skull as electrical fields are, leading to a higher spatial resolution for MEG.

Estimating the spatial extent of the source could help the neurosurgeons to remove the right volume of the brain without causing functional loss. On the other hand, an interictal spike may propagate rapidly in the brain along the cortical surface. The region of interest is the onset of the epileptic discharge. Without information on the temporal behavior of the source, the propagation zone may be mistaken for the spike onset zone. Therefore, one needs a source localization technique able to accurately assess the spatio-temporal evolution of the underlying generators.

MEG source localization is an inverse problem aiming at reconstructing the neural activity producing the MEG data. Different localization approaches have been proposed [38, 77]. Distributed source localization, which is discussed in this thesis, is based on the assumption that the MEG signal is produced by a set of evenly distributed generators on the cortical surface. The problem is ill-posed: an infinite number of configurations of the generators inside the brain can give rise to the same MEG signal outside the head. Therefore additional information should be added to find a unique solution. Our laboratory developed a source localization

technique entitled Maximum Entropy on the Mean (MEM) which assumes that the brain is acting as a set of parcels that can be active or not [2, 36]. This method was proven to be sensitive to the spatial extent of the source of epilepsy in EEG [36] and in MEG [16].

The objective of this master's project was in direct continuity with the work of Rasheda Chowdhury, a former Master student and current PhD student under the supervision of Dr Grova. Her master's thesis [15] and her published article [16] aimed at evaluating the ability of distributed source localization methods to localize accurately spatially extended sources of brain activity in MEG. Assessing the size of the brain region involved in the generation of the interictal spike is of great interest during the presurgical investigation of patients with epilepsy. She showed, based on simulated data, that the maximum entropy on the mean technique (MEM), a source localization technique developed in the laboratory [2, 36], was sensitive to the spatial extent of a source. MEM source reconstruction depends on a spatial clustering of the brain: Chowdhury proved that the size of the parcels of the clustering did not affect the spatial performance of the MEM reconstruction.

The present master's project is organized in three parts. The goal of the first one was to evaluate the accuracy in estimating the time course of underlying sources in MEM source localization with realistic simulations of interictal spikes. The second part aimed at characterizing the spatial resolution of the MEM operator, by estimating its resolution matrix. Finally the last part consisted in

proposing a statistical method dedicated to the implementation of a statistical map of activation.

In previous studies from our group, only spatial accuracy at the peak of the simulated spike was considered. The evaluation of the spatial extent was based on the area under the receiver operating characteristic (ROC) curve (AUC) at the peak of the signal, which is a detection accuracy index. My first objective consisted in evaluating the ability for the MEM technique to reconstruct the time course of a propagating interictal spike. If an interictal spike propagates along the cortical surface, the estimation of the propagation pattern is needed to identify clearly the onset of the propagation. Assessing the accuracy of temporal time courses reconstructed within the MEM framework is actually far from trivial. Most source localization techniques, as explained in Section 3.2.1, can be viewed as linear filter converting data from the sensor space to the dipolar generator space. However since they are linear, the temporal behaviour is usually reflecting the time course of the signal selected for source localization. On the other hand, MEM is nonlinear, which makes the estimation of the time course more challenging, since MEM estimation is done for each time sample independently.

We were wondering if MEM approaches were able to estimate the spatial extent of a source. To do so, assessing the spatial accuracy of the MEM operator per se was an important issue. One way to address this issue is to analyze the resolution matrix, which describes how well sources can be estimated [62]. An analytical formula to compute the resolution matrix exists for linear source localization. However, for MEM technique, such a solution is not available.

However it is possible to estimate the resolution matrix, by calculating the point spread functions for each dipole along the cortical surface.

The third part of my Master's project consisted in the development of a statistical map of active generators. So far, the result of the MEM techniques was a map of estimated current densities of the generators on the cortical surface along time. Since we have demonstrated that MEM was sensitive to the spatial extent of the source, our objective was to provide an estimate of the actual spatial extent of the underlying generators. The method proposed in this thesis aims at defining a test statistic for each generator, using a non-parametric resampling approach.

Chapter 2 introduces the state of the art in the domain of electrophysiology, epilepsy and MEG source localization. Chapter 3 presents the study of the temporal and spatial accuracy of the MEM techniques. The MEG source localization technique is compared to a standard technique, the minimum norm estimate (MN) [38], with realistic simulation of interictal spikes which propagate along the cortical surface. The resolution matrices of MN and MEM are compared in Chapter 4. Our goal was to quantify the spatial resolution of both source localization techniques. In Chapter 5, a new bootstrap-based statistical analysis is proposed and discussed. We aimed at estimating of map of activation base on the reconstructed amplitude of the generators. Finally, a global discussion and conclusion are presented in Chapter 6.

Chapter 2
State of the art of source localization with magnetoencephalography in the context of epilepsy

2.1 Electrophysiology of the human brain

Neurons are brain cells that convey information via electrical or chemical signals. There are about 50-100 billion neurons. As depicted in Figure 2–1, a neuron is typically composed of dendrites which receive information from other neurons: the soma where the electrical inputs are processed, and one or several axons which represent the output structure of the cell. Very often, the axon is covered by a myelin sheath which facilitates the transmission of the electrical signal along the axon.

One can distinguish between different types of neurons. The most important ones for EEG/MEG recordings are the pyramidal cells. They are found within the layer V of the cortex, as well as in the hippocampus and in the amygdala. They play important roles in numerous cognitive functions. They are denoted as pyramidal because of the triangular shape of their soma (see Figure 2–2). They are composed of multiple dendrites and a single axon, both dendrites and axons branch extensively. They are more often excitatory, i.e. when activated they provoke a depolarization in efferent neurons.

The information communicates between neurons through the synapses. There are around 100 trillion synapses in the nervous system. A synapse is a

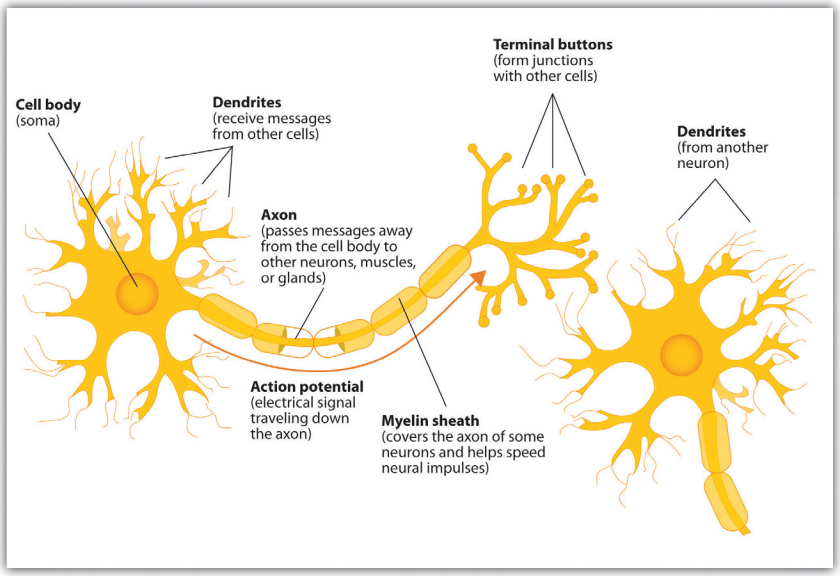

Figure 2–1 – Components of a neuron. Taken from [82]

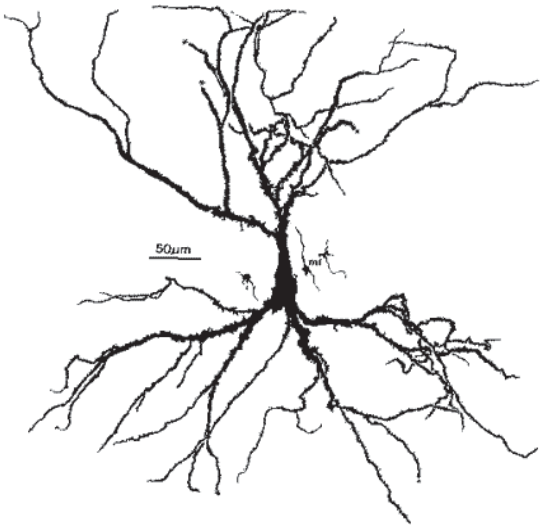

Figure 2–2 – A pyramidal neuron in the hippocampus. Taken from `wikipedia.com`

junction between two neurons, most of the time from an axon to a dendrite. The function is unidirectional: the information only goes from the so-called presynaptic neuron to the postsynaptic neuron. In most cases, the transmission of information in a synapse is assured by chemical messengers called neurotransmitters and the principle of a synapse activation is explained in Figure 2–3. A synapse is composed of a presynaptic terminal, the end of the axon of the presynaptic neuron; the postsynaptic terminal, where the afferent neuron will receive the neurotransmitters; and a gap between the two, called the synaptic cleft. The neurotransmitters are stored in the presynaptic terminal, in vesicles inside the cell. The release of the neurotransmitters is done when an action potential, a neuronal event caused by the soma, depolarizes the presynaptic terminal. The change of polarity of the membrane cell activates the voltage-gated calcium ion Ca^{2+} channels. The Ca^{2+} channels open, which causes a movement of calcium ions into the neuron. The Ca^{2+} inside the presynaptic terminal induces the fusion of the vesicles with the neuron membrane - the neurotransmitters are then released into the synaptic cleft. These chemical agents bind with the receptor molecules in the postsynaptic membrane, which cause the opening and closing of different ion channels (mainly Na^{+}, Cl^{-} and K^{+} ions). This produces a displacement of charges: the postsynaptic potential (PSP). A PSP can be either excitatory or inhibitory, depending on whether the exchange of ions between the cell and the extracellular medium creates a depolarization (for excitatory neurons) or a hyperpolarization (for inhibitory neurons) of the membrane cell. The neurotransmitters which did

not bind to the postsynaptic neuron are taken up by the presynaptic cell, and new vesicles are created.

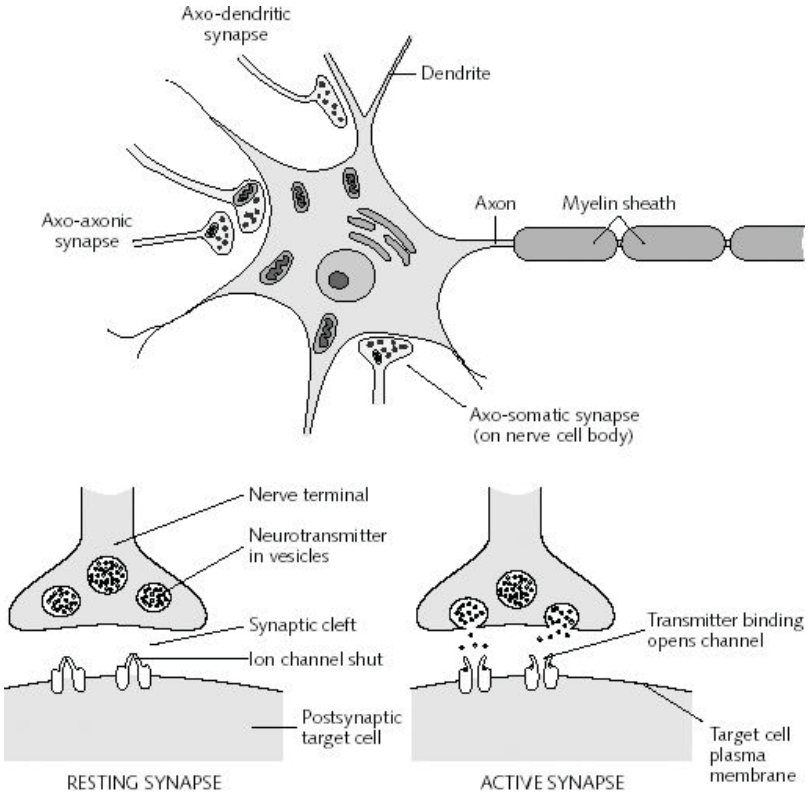

Figure 2–3 – Functioning of a synapse. Taken from `http://www.answers.com/topic/synapse`

Excitatory postsynaptic potentials (EPSPs) last from 10 to a few hundred milliseconds with an amplitude of 10 mV. If several EPSPs are involved in a short period of time, the PSPs are summed and the change in the membrane potential would therefore be larger. If a neuron receives two EPSPs from synapses that are near each other, their postsynaptic potentials are added together. The resting membrane potential is -70mV. If enough EPSPs are engaged, and the membrane

potential reaches a threshold around -55mV, an action potential (AP) is created. An AP is an event lasting a few milliseconds, of high amplitude which propagates along the axon. On the other hand an inhibitory PSP provokes a hyperpolarization of the membrane below -70mV, which limits the production of APs.

EEG and MEG sensors are mainly sensitive to the PSP of the pyramidal cells located in layer V of the cortex [67]. The PSPs provoke a difference of electric potential between the apical dendrite and the soma of the cell. This induces a movement of ions within the dendrite trunk, and therefore a current, which is called the primary current. Others currents with direction opposite to the primary current will flow in the extracellular medium to ensure the conservation of electric charge. Those are called secondary currents or volume conduction. If a large population of pyramidal cells (at least 100,000 neurons) is recruited synchronously, the current dipoles generated by all dipoles with similar orientation (perpendicular to the cortical surface) sum up, and create a signal of sufficiently large amplitude that could be recorded from the scalp using EEG or MEG. (Figure 2–4).

The post synaptic currents create both an electric field and a magnetic field, which can be recorded using EEG and MEG respectively. The two fields are orthogonal to each other: the magnetic field rotates around the main direction of the current (see Figure 2–5).

2.2 Epilepsy

An **epileptic seizure**, according to the definition proposed by the International League against Epilepsy and the International Bureau for Epilepsy, is "a transient occurrence of signs and/or symptoms due to abnormal excessive or

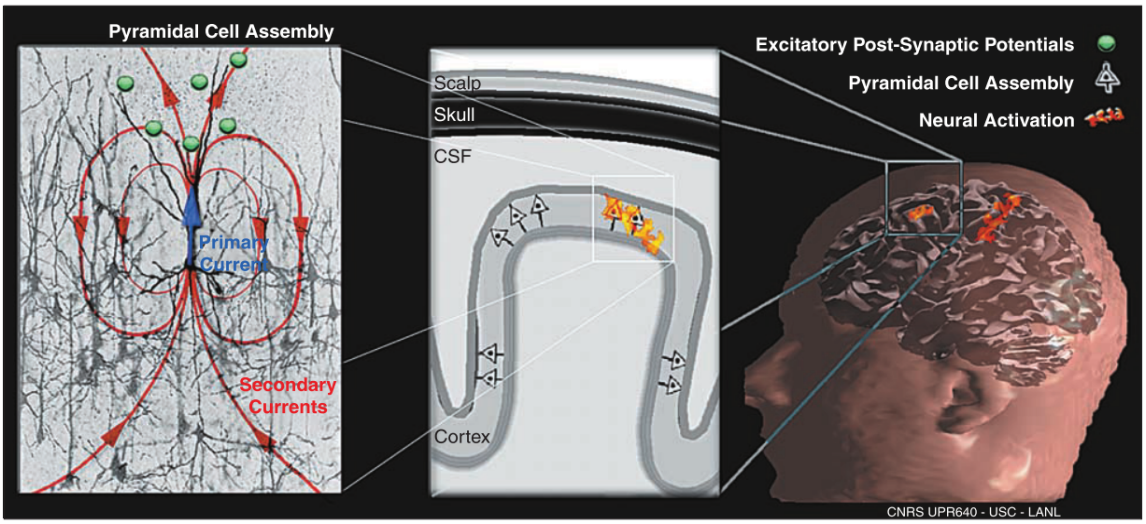

Figure 2–4 – Generation of the EEG or MEG signal. Left: the primary current on a pyramidal cell is due to the appearance of excitatory post synaptic potential on the dendrite of the cell. The law of conservation of energy tells us that other currents must flow in the direction opposite to that of the primary current to obtain a closed current loop. While the primary current is intracellular, the secondary currents flow through the volume conductor. Centre: the pyramidal cells are located on the cortical surface and are all oriented normal to the cortical surface. Right: a large population of neurons is necessary to obtain an EEG or MEG signal. Taken from [3]

synchronous neuronal activity in the brain". **Epilepsy** "is a disorder of the brain characterized by an enduring predisposition to generate epileptic seizures and by the neurobiological, cognitive, psychological, and social consequences of this condition. The definition of epilepsy requires the occurrence of at least one epileptic seizure" [29].

Epilepsy is not a disease, but rather a condition of the brain where a sudden and abnormal neuronal discharge could occur, provoking a seizure. This disorder can be caused by different factors, which is the reason why some researchers in the

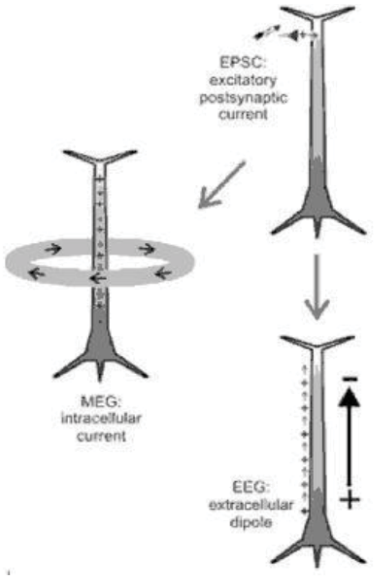

Figure 2–5 – Primary source of MEG and EEG. Taken from [48]

domain prefer the term *epilepsies*. Seizures can be due to anatomical anomalies, malformations of cortical development, brain lesions, tumours, central nervous system disease, post-traumatic scar or other abnormalities (whose cause may not be known or identified) [27].

There are three main features characterizing an epileptic seizure [29]:

- It is demarcated in time, delimited by a clear onset and termination. Typically, a seizure lasts a few minutes, but can be as short as a few seconds. On the other hand, a long-duration case of epileptic seizures, called *status epilepticus*, can last days or weeks.
- It provokes clinical manifestations. Those clinical signs are various, depending on the location of the brain areas involved during the generation and

propagation of the seizure. Epileptic seizures can involve loss of consciousness; interruption of memory; sensory, visual or auditory hallucinations; motor automatism such as jerking; change of emotional state, etc. Not all seizures affect all of these factors and patients can experience seizures causing different clinical signs.

- It is caused by an abnormal synchrony of overexcited neurons in a region of brain. This excessive and unpredictable discharge is often due to a decrease in local inhibition on a population of pyramidal neurons. These abnormal neuronal discharges gave rise to changes in electro-magnetic activity in the neurons, that can most of the time be detected remotely by measuring differences of electrical potentials using scalp electroencephalography (EEG) and variations in magnetic field with magnetoencephalogaphy (MEG). This concept is developed in section 2.1. It is worth noting here that some epileptic events provoke long-lasting abnormal discharges detectable by EEG, but without causing any clinical signs. These types of events are called electrographic seizures.

Epileptic seizures can be classified into two main categories. If the seizure onset zone is a delimited brain region, the epilepsy is referred to as focal or partial epilepsy. On the other hand, generalized seizures involve extended brain regions over both hemispheres. Focal seizures can be simple or complex, depending on whether they are associated or not with a loss in consciousness and memory [30]. Focal seizures can propagate through all the brain and become secondary generalized events.

One type of generalized seizure is absence seizure, which is characterized by a brief loss of consciousness along with staring spells lasting seconds. On the other hand, tonic-clonic seizures are generalized seizures which involve an impairment of consciousness following stiffening (tonic activity) and rhythmic jerking (clonic activity) of the limbs.

Epilepsy affects 1% of the population in Canada [91]. Epileptic seizures can be controlled through long-term drug therapy. Medication does not cure epilepsy but helps to reduce or stop the occurrence of seizures. The type of medication prescribed to the patients depends on the type and the frequency of the seizures and the patient's age and condition. However, 30% of the patients are drug-resistant, meaning that medication has no or little effect on the symptoms. For those patients, other forms of treatments are considered. Patients with focal epilepsy may undergo surgery to resect the brain region responsible for the seizures while avoiding any important functional loss.

Table 2–1 reports the definition of all the regions of interest in the brain in the context of epilepsy. The *epileptogenic zone* is the part of the brain epileptologists need to identify. There is no direct measure to detect this zone. However, it is possible to detect areas in the brain which are involved in epilepsy and related to the *epileptogenic zone*.

EEG and MEG allow the detection and localization of the generators of the interictal spikes and seizures, which correspond to respectively the *irritative* and *ictal onset zone*. An interictal spike is a transient event characterized by abnormal neuronal discharge. The interictal spikes can become visible on scalp EEG and

Table 2–1 – Brain areas of interest in partial epilepsy. Taken from [27]

Brain area	**Definition**	**Measure**
Irritative zone	Area of cortex that generates interictal spikes	EEG
Ictal onset zone	Area of cortex that initiates or generates seizures	EEG
Epileptogenic lesion	Structure pathology of the brain that is the direct cause of seizures	CT, MRI, tissue pathology
Symptomatogenic zone	Portion of the brain that produces the first clinical symptoms	EEG, behavioral observation
Functional deficit zone	Cortical area producing nonepileptic dysfunction	Neurologic exam, neuropsychology, PET, SPECT
Epileptogenic zone	Total area of the brain that is necessary to generate seizures and that must be removed to abolish seizures	Unknown

MEG as soon as they involve an extended portion of the cortex in order to generate a signal of sufficient amplitude to be detected from ongoing background. The interictal spike is not associated with any clinical manifestation; the patient is not even aware when the discharges occur. In practice, it is more frequent and convenient working with interictal spikes: they happen more frequently than seizures. Also, patients move during seizures, provoking motion artifacts. This makes the analysis of the data of EEG or MEG more challenging. Both the *irritative* and *ictal onset zones* are believed to be very close to the *epileptogenic zone*.

When epileptic seizures are likely to be generated by an underlying lesion, the area of the lesion may be detected with brain imaging techniques such as Magnetic Resonance Imaging (MRI) [9, 83] and computed tomography (CT) or with the analysis of tissue pathology. These techniques reveal the *epileptogenic lesion*, whose resection is often enough to abolish epileptic seizures.

Sometimes, patients with epilepsy may have a deficit in cognitive functions. The location in the brain of those malfunctioning functions (the *functional deficit zone*) can help to localize the *epileptogenic zone*. For this, neurological and neuropsychological exams are used to help to define the impaired cognitive functions. They can also be localized using neuroimaging techniques following brain metabolism and perfusion such as position emission topography (PET) [50] and single-photon emission computed tomography (SPECT) [88].

2.2.1 Localization of the generators of interictal spikes

EEG and MEG interictal spikes are large amplitude spontaneous discharges that can be detected from background EEG/MEG activity only when the underlying generators correspond to the synchronization of the discharges of a spatially extended area. Studies have suggested that a cortical area of at least 4cm^2 should be active to be detected in MEG [86]. Similar studies have suggested an area of 6 to 10cm^2 is needed to be able to detect a spike in scalp EEG [72].

To detect interictal spikes, expert epileptologists examine EEG/MEG recordings and identify abnormal events following the criteria outlined by Walczak et al. [90]:

1 The waveform should be clearly distinguished from the background activity.

2 It should be a spike, i.e. there must be a abrupt and rapid change in polarity.

3 It should last between 30 and 200 milliseconds.

4 It should be physiologically plausible, unlike EEG artifacts. Practically, it means that if the spike is recorded by more than one electrode, it must have a voltage gradient across the scalp.

It is worth noting that these criteria were proposed for EEG. So far, no equivalent has been proposed for MEG recording.

One of the advantages of EEG and MEG is that they provide a map of activity of the whole cortical surface. Also, they are non-invasive, meaning that no electrodes are implanted inside the head. Invasive recordings, such as intracranial EEG, are used in epilepsy if non invasive studies do not succeed in giving a clear location of the epileptogenic zone. One can use either a grid of electrodes

placed on the cortical surface or depth electrodes that can reach deeper structures (such as hippocampus or amygdala). As in situ invasive recordings, intracranial EEG recording allows one to acquire data with excellent signal to noise ratio. However they only give an indication of a local area in the brain. Indeed, due to the invasiveness of the procedure, only few intracranial electrodes can be implanted, thus limiting the spatial coverage. This is why EEG and MEG should be considered to guide the implantation of invasive electrodes, to make sure placing them near the irritative zone [84].

Interictal spikes are spontaneous events that, besides involving an extended brain region, can also propagate. Several studies have investigated the propagation of interictal spikes, especially for temporal lobe epilepsy [47, 85, 5]. Different patterns have been identified: for example from mesial to a lateral temporal location [24], or from anterior to posterior temporal region [26]. It is commonly accepted that the propagation is due to the activation of a neural network by the group of cells triggering or propagating a spike. The delay between the two spikes along the propagation depends on the level of myelinisation of the track connecting the populations. The speed of the connectivity can vary from 1m/s to 40m/s [26].

An accurate characterization of the propagation patterns is required during the presurgical evaluation of patients with epilepsy, because the detection of the first region where the spike is generated allows the neurosurgeons to better estimate the brain region to resect. Accurate characterization of the propagation patterns of interictal spikes are related to the good outcome of epilepsy surgery because the irritative zone, i.e. the onset of the interictal spike, is more likely to be

identified correctly [85, 56, 40]. In Lantz et al, 2003[56], the authors warn the users of EEG and MEG source localization algorithms that not taking into account spike propagation can lead to wrongly localized results.

Several studies have shown that MEG has a better ability to detect propagation than EEG [40, 42, 85]. This can be explained by a better spatial sensitivity of MEG and a higher signal to noise ratio (SNR) in the lateral temporal and frontal cortex. The superior spatial accuracy of MEG is due to the influence of the skull on the electric fields generating the EEG signal. The low conductivity of the skull tends to distort the electric fields, thus reducing the spatial accuracy of EEG [6] while the skull has almost no impact on MEG data.

2.2.2 Other modalities for localization

All the localization techniques can be classified according to their temporal and spatial resolution. For example both EEG and MEG have the advantage of a very high temporal resolution (about 1ms) but a poor spatial resolution (5 to 20mm after source localization, depending on the brain area). As shown in Figure 2–6, most other non invasive modalities offer a better spatial resolution.

Whereas EEG and MEG directly measure neuronal activity, i.e. neuronal bioelectrical activity, other modalities indirectly estimate brain activity.

The principle of functional Magnetic Resonance Imaging (fMRI) consists of detecting the changes in blood oxygenation and flow that occur in response to neural activity. Since hemoglobin is diamagnetic when oxygenated (oxyhemoglobin) but paramagnetic when deoxygenated (deoxyhemoglobin), one can observe small changes in the magnetic resonance signal depending on the level of oxygenation.

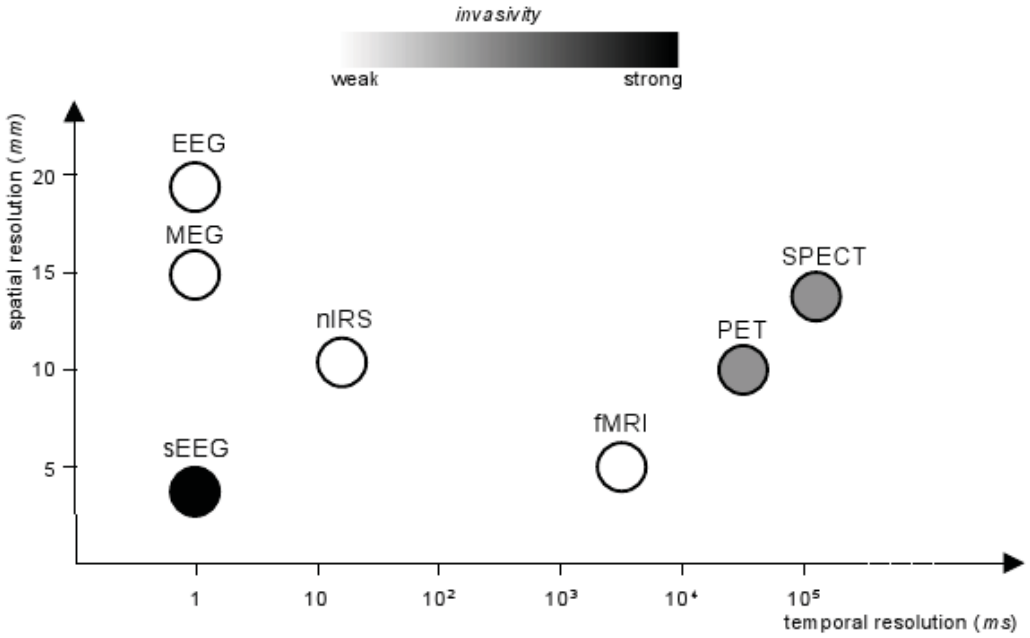

Figure 2–6 – Spatiotemporal resolution and invasivity of brain functional imaging modalities. Taken from [34]

The underlying theory is that an active brain area consumes more oxygen. Therefore, the blood-oxygen-level dependent (BOLD) signal recorded by the fMRI correlates with neural activity [71]. It is also possible to record simultaneously EEG and fMRI. Then, EEG is used as a trigger for studying epileptic activity: once an epileptic discharge is detected in EEG data, the hemodynamic response is inspected few seconds afterward [33].

Positron emission tomography (PET), as well as single photon emission computed tomography (SPECT), focus respectively on the glucose consumption and the cerebral blood flow (CBF), both indirect indicators of neuronal activity. These techniques are slightly invasive because they require the injection of a

radioactive tracer. SPECT can be used during an epileptic seizure (ictal SPECT) to measure CBF during the first moments of a seizure. The goal is to inject radioactive tracer as soon as the first signs of a seizure appear [51].

Similarly to fMRI, near-infrared spectroscopy (NIRS) measures local changes in hemodynamic activity, exploiting specific absorption spectra of oxy- and deoxy-hemoglobin in the near infra-red, using optic fibers placed on the skin [10]. EEG is used to identify the epileptic discharges, while NIRS is used to monitor local fluctuations of oxy- and deoxyhemoglobin elicited by the discharge [60].

Most of the time, noninvasive methods are sufficient to evaluate the patients before surgical resection. However, if these techniques do not detect the epileptogenic zone accurately enough, intracranial EEG investigation is considered [70]. Different techniques exist; the choice of the type of electrode to implant and its location depend of the type of epilepsy of the patient. Hence, a specific implantation planning has to be tailored on a case by case basis.

2.3 Electroencephalography (EEG)

2.3.1 History of EEG

Electroencephalography was first recorded in human by the German physiologist Hans Berger [37]. He did his first experiment on his son, described alpha and beta rhythms in the brain and invented the term 'electroencephalogram'. Hans Berger was able to record signals to the order of microVolts with a string galvanometer. The first EEG recording are shown in Figure 2–7.

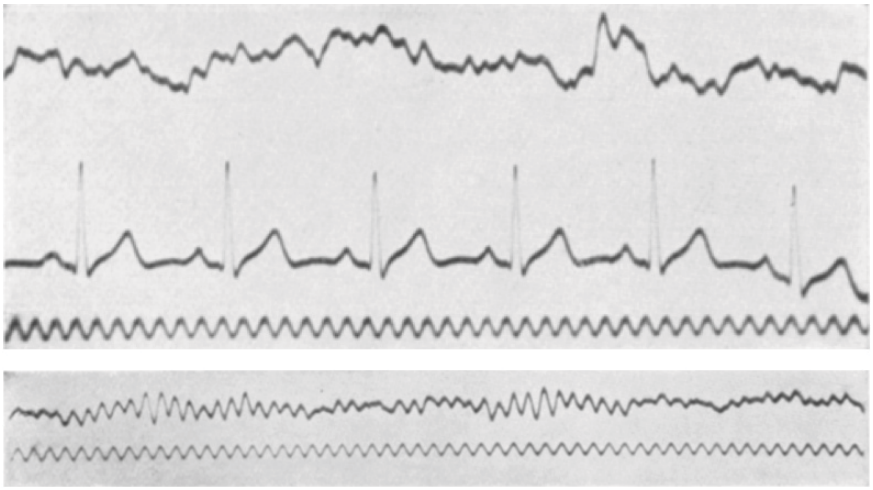

Figure 2–7 – The first reports of the human EEG from the first publication from Hans Berger. **Top:** top line represents beta wave activity, related to normal waking consciousness; the middle tracing is the ECG and the lowest tracing is a generated 10 Hz sine wave. **Bottom:** top line shows what is known now as alpha rhythm which happens when the subject's eyes are closed. The lowest tracing is a generated 10 Hz sine wave. Taken from [8]

2.3.2 Instrumentation for EEG

EEG records brain electrical activity by placing electrodes along the scalp. In a modern EEG system, the electrodes are connected to an amplifier and the signals are then digitized and stored on a computer. Signals measured by EEG sensors have an order of magnitude in the range of a few μV.

A standardization electrode placement scheme, the 10-20 system, was proposed by Jasper in 1958. It has permitted a congruence among the laboratories around the world and helped the development of this technique. This system is based on 10% or 20% proportional distances along a longitudinal line of the head between two anatomical landmarks (nasion and the inion) as well as along a transverse line of the head between the left and right pre-auricular points. The nasion

is the intersection of the frontal and two nasal bones of the human skull, and the inion is the most prominent projection of the occipital bone at the posterioinferior (lower rear) part of the skull. The standard recording array for adults consists of 21 electrodes plus a ground electrode, as seen in Figure 2–8(A,B). Each electrode is specified by a letter name related to the general underlying cortical region or lobe (frontopolar - Fp; frontal - F; temporal - T; occipital - O; parietal - P) and a subscript reflecting its position relative to the midline. Even and odd numbers refer to the right and left hemispheres respectively, and the z (zero) refers to an electrode placed on the midline. When recording a more detailed EEG with more electrodes, extra electrodes are added in the spaces between the existing 10-20 systems (Figure 2–8(C)). Nowadays, most research protocols use 19 to 64 electrodes, but can reach as many as 512 electrodes.

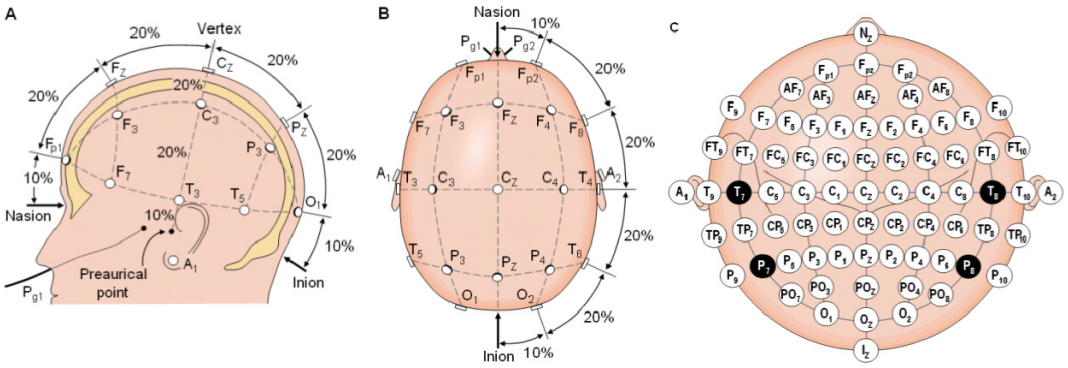

Figure 2–8 – The international 10-20 system seen from (A) left and (B) above the head. A = ear lobe, C = central, Pg = nasopharyngeal, P = parietal, F = frontal, Fp = frontal polar, O = occipital. (C) Location and nomenclature of the intermediate 10% electrodes, as standardized by the American Electroencephalographic Society. Taken from [81]

2.4 Magnetoencephalography (MEG)

2.4.1 History of MEG

The first human magnetoencephalography signal was measured by Dr David Cohen in 1968 [17]. MEG signal was recorded using a single copper induction coil at the University of Illinois. To avoid environmental noise (such as electrical devices, elevators, cars, or even the Earth's steady field), the MEG was recorded in a shielded room. The signal to noise ratio increased drastically thanks to the invention of superconductive quantum interference device (SQUID), an ultrasensitive detector of magnetic flux, developed by Dr Zimmerman [96]. Figure 2–9 shows the signal of the first MEG recorded with SQUID in Massachusetts Institute of Technology.

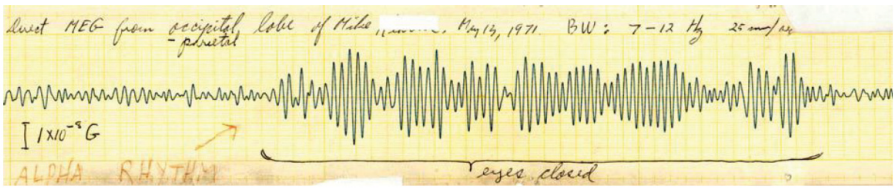

Figure 2–9 – First MEG signal recorded with a SQUID in May 1971, in a shielded room in MIT. One can clearly see the apparition of alpha rhythm when the subject closes his eyes. Taken from [18]

From the first single-sensor recording, the number of sensors has progressively increased to reach around 300 MEG sensors organized within a helmet for MEG devices available nowadays. In present-day systems, all the sensors are placed in a helmet for a faster and a more efficient recording. Figure 2–10 shows a picture of a MEG system.

Figure 2–10 – A MEG system. Taken from wikipedia.

2.4.2 Instrumentation for MEG

The neuronal signal recorded by MEG is of very low amplitude. The magnetic fields corresponding to brain activity are of the order of femto (10^{-15}) to pico (10^{-12}) Tesla. For comparison, the Earth's magnetic field is of the order of 10^{-4} Tesla. All electronic, as well as cars and elevators produce a field of order of microTesla. For these reasons, in order to record MEG data, one needs the combination of three main elements:

- **Ultrasensitive detectors.** To detect magnetic fields, induction coils are generally used. A variation of magnetic flux through a coil composed of one or several loops will generate an electric current in the coil: the principle is called magnetic induction. However, the detection of brain magnetic field with a regular coil is almost impossible; one would record almost nothing, as all the energy would be dissipated in heat due to the inherent

resistance of the coil. This is why we use a supraconductive environment to reduce at the maximum the resistance of the materials. For that reason, the induction coils used to detect fluctuations of the magnetic field are coupled with superconducting quantum interference devices (SQUIDs) which are very low noise, ultra high gain, current-to-voltage converters. To allow supraconductivity, the coils and the SQUIDs are placed in liquid helium, at a temperature of 4 ° K (-269 ° C).

There are two types of MEG sensors: magnetometers and gradiometers. The magnetometer consists in only one coil placed as close as possible to the head of the subject (see schema in Figure 2–11 (a)). It offers the advantage of being very sensitive to the magnetic field, however it is also sensitive to environmental magnetic noise. The gradiometers are made of two magnetometers or more wound in an opposite sense separated by a certain distance. The gradiometers measure the difference of magnetic fields recorded by the two coils. There exist different configuration of gradiometers, and the most commonly used is the radial gradiometer as illustrated in Figure 2–11 (b). As we can assume the ambient noise is the same on both coils, gradiometers cancel out those distant sources of noise. On the other hand, gradiometers are less sensitive to deep sources than magnetometers.

– **A shielded room.** To get rid of the environmental noise (including the Earth's magnetic field), the MEG is placed in a shielded room, which

is generally constituted of nested layers of aluminum and mu-metal, a nickel-iron alloy.

– **Reference sensors.** Even in a shielded room, there are still magnetic fields interfering with the MEG signal. They may be due to some remaining environmental noise, instrumental noise and activity coming from the body of the subject himself. The heart, for instance, produces a magnetic fields 1000 times stronger than brain activity. To remove this noise, which is considered identical within the whole room, some MEG devices are equipped with reference sensors that consist of magnetometers and gradiometers centimeters away from the head of subject. Those sensors record ambient noise while taking into account the fixed geometry between the reference sensors and the sensors of interest.

2.5 EEG and MEG source localization

Both EEG and MEG consist in scalp recordings, offering thus very weak spatial resolution. The goal of source localization for EEG and MEG modalities in the context of epilepsy is to localize the generators of the electromagnetic fields measured at the time of neuronal epileptic discharges. The physics of these fields is described by Maxwell's equations.

The first step of source localization is to solve the forward problem. This consists in computing a model that describes how a dipolar current source in the brain will contribute to the signal measured outside the head using EEG electrodes or MEG sensors.

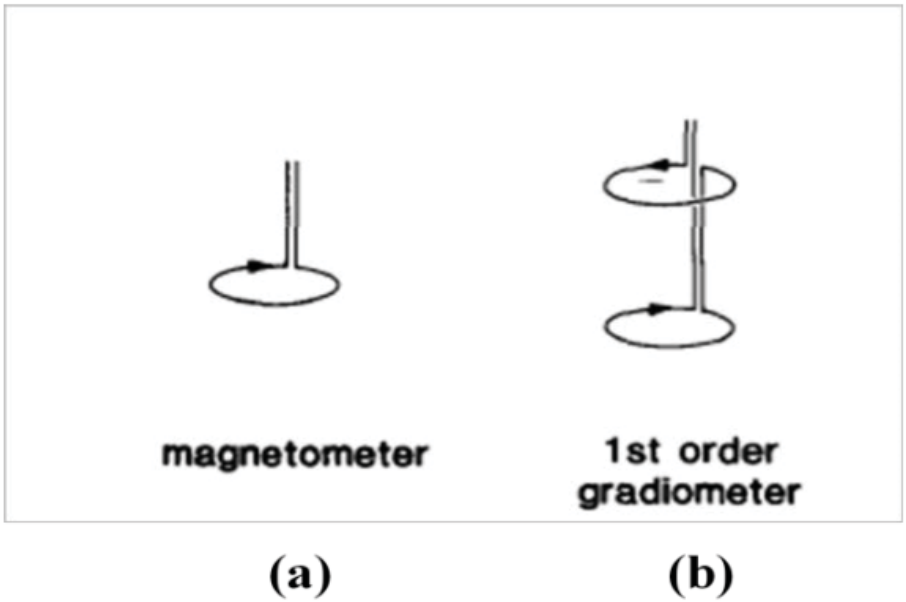

Figure 2–11 – Commonly used MEG sensor configurations. (a) magnetometer (b) 1st order gradiometer. Taken from [41]

The solution of the forward problem is needed to solve the inverse problem, the actual goal of source localization, that is to say finding within the brain the generators of some specific activity measured using EEG and/or MEG. The forward and the inverse models are illustrated in Figure 2–12.

2.5.1 The forward problem

In order to compute the EEG and MEG signals generated by a known distribution of sources, it is necessary to choose a head model and to make some assumptions and simplifications about the source and volume conductors. The forward model is then solved using Maxwell's equations, which describe how electric charges and electric currents act as sources for the electromagnetic field. Since the useful frequency spectrum for electrophysiological signals in MEG and

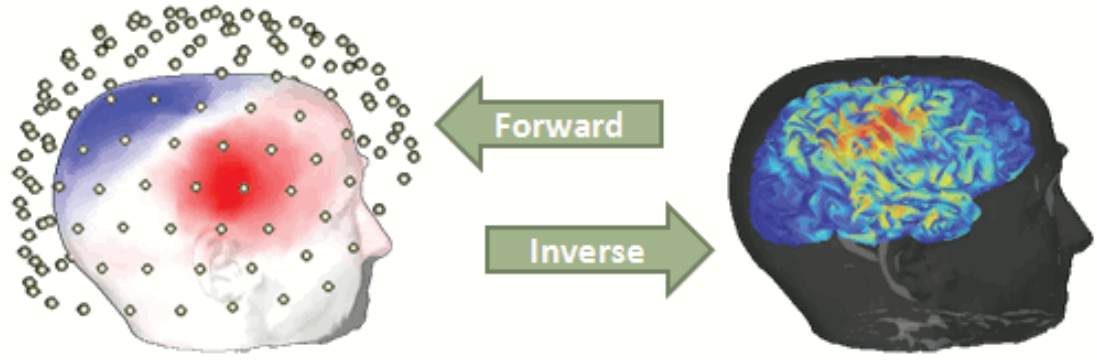

Figure 2–12 – Forward and inverse models for MEG data. Taken from `http://neuroimage.usc.edu/brainstorm/Tutorials/TutHeadModel`

EEG is typically below 1kHz, the electromagnetic field is calculated within the quasi-static approximation of Maxwell's equations.

The head geometry can be modeled as a set of nested concentric homogeneous spherical shells representing the brain, the skull, the scalp and possibly the Cerebro Spinal Fluid (CSF) compartment of a human head. This simple geometry allows one to reduce the Maxwell's equations to provide an analytical solution to the problem, thus easier to compute [78]. EEG studies have shown that such simplified models cannot produce satisfactory results [13] since the electric fields are very sensitive to the anatomy of the skull. Indeed the skull is very resistive compared to the surrounding tissues (the skin and the cortex), therefore the electric fields tend to smear spatially. This is the reason why one needs to model the skull accurately enough to take this phenomenon into account. MEG data analysis is much less impacted by this simplification [45] since magnetic fields are not affected by the resistivity of the skull. In spite of that, the spherical head

model is still routinely used in most clinical and research applications for EEG and MEG source localization.

More accurate solutions to the forward problem use anatomical information obtained from high-resolution volumetric brain images obtained with MRI. The 3D representation of the brain, the skull and the scalp are extracted from the images. A boundary element method (BEM) can be used for the calculation of the forward solution, which takes into account only the surfaces between the regions, assuming homogeneity and isotropy within each region [54, 65]. A more accurate method is the finite element method (FEM), which considers all the volume and can deal with local inhomogeneities [92]. Both BEM and FEM are very powerful approaches to solve the forward problem but are very time consuming [3].

The main difficulty for EEG is to initialize the conductivity values of the brain, the skull and the scalp. Indeed, the estimation of these values might be erroneous, as they are done in animal studies, or post mortem.

Since MEG is less affected by the conductivity, the computation of the forward model for MEG is easier. For this work, we will use a 1-layer BEM model, modeling only the inner surface of the skull, assuming that the magnetic permeability is the same for the skin, the skull and the brain. BEM offers a good trade-off between the realism and the complexity of the model. The forward model is calculated with OpenMEEG software [35, 54]. One main advantage of the software is that it is able to solve the issue of numerical instabilities when generators are located too close to the BEM surface.

2.5.2 The inverse problem

To estimate the neural sources of EEG or MEG data, three types of general approaches are used: parametric model, dipole scanning approach and distributed sources model.

The parametric model assumes that the measured data have been produced by a few generators and each of them can be modeled using an equivalent current dipole (ECD). The number of ECDs is fixed. The unknown parameters are then the location, the orientation and the amplitude of these dipoles. Some of these parameters can be fixed to facilitate the solution of the problem. The three principal dipole models are: the *rotating dipoles*, with fixed position, the *fixed dipoles*, with fixed position and orientation, and the *moving dipoles*, with all the parameters unknown [79]. The main limitation with these methods is that the user has to fix a priori the number of dipoles. For these reasons, dipole fitting approaches are commonly used with only one dipole, or sometimes a few, after one is set to a known position. These limitations imply that such methods can only be used reliably with one or few very focal active regions. This is usually a valid assumption for brain activations occurring shortly after stimulation of primary functions (somatosensory, auditory or visual) [34]. However, the ECD model can also provide misleading results when the source of activity is too spatially extended [52], leading to inaccuracy in the estimation of the depth of the ECD.

Dipole scanning approaches focus on a region of interest, for example a regular grid within the brain. An estimator of the contribution of each putative source location to the data can be derived either via spatial filtering techniques

(beamforming approach, [89, 14]) or signal classification indices (Multiple Signal Classification approach (MUSIC), [66]). Historically these scanning methods were first introduced in the radar and sonar community. An attractive feature of this method is that they do not require any a priori on the number of underlying sources. However, they make the strong assumption that the activations of the different sources are uncorrelated. As a dipolar model evaluated iteratively on each point on the grid, dipole scanning approaches could not be sensitive to the spatial extent of the generators.

The distributed sources to model the MEG/EEG inverse problem consist of considering the cortex as a set of distributed dipoles at fixed locations along the cortical surface thus allowing to incorporate realistic anatomical constraints to regularize the ill-posed inverse problem [22]. In this case, since the locations are fixed, only the linear parameters, i.e. the current density, need to be estimated, and the inverse problem reduces to a linear one with strong similarities to those encountered in image restoration and reconstruction.

Typically, the dipolar sources are placed at each node of a triangular tessellation of the surface of the cortical layer, obtained by anatomical MRI. Assuming the pyramidal cells are organized perpendicularly to the cortical layer, we can constrain each of these dipoles to be normal to the surface, which permits to reduce by 3 the degrees of freedom of the model. However, a good representation contains thousands of dipole sources, and the number of sensors is generally only few tens for EEG and few hundreds for MEG. Therefore, the inverse problem is largely underdetermined and needs constraints or prior information to be solved.

The most common ways to regularize the inverse problem is to consider the solution with the minimum energy (Minimum Norm Estimate (MNE) [45]), or with the maximum spatial smoothness (Low Resolution Electromagnetic Tomography (LORETA) [77]). Others techniques, using Bayesian probabilistic approach [87] or the Maximum of Entropy on the Mean (MEM, [36]), have been proposed. Bayesian and MEM techniques provide a framework where you can add any prior information. This gives the flexibility of choosing the constraint to regularize the inverse problem, and also allows the possibility to compare models.

Chapter 3
Spatio-temporal evaluation of reconstructed propagating sources

3.1 Rationale

The localization of the EEG and MEG sources is a challenging topic, and many researchers proposed methods to solve this inverse problem [38, 21, 77, 20, 76, 36]. From our group, Amblard and colleagues developed a source localization method based on a data-driven parcelization of the brain, and a non-linear regularization maximizing the μ-entropy [2]: the maximum of Entropy on the Mean (MEM). It showed the good performance of the method and demonstrated that, unlike standard linear techniques, MEM was sensitive to the spatial extent of the source [36, 16], which makes it an interesting source localization technique, especially for spatially extended sources (such as the generators of interictal spikes).

However, the temporal accuracy of the reconstruction of the MEM method has never been studied. Whereas providing an accurate estimate of the time course of underlying source is of great importance for any source localization method, it is particularly important in the context of epilepsy to localize the onset of propagating discharges. To analyze its temporal accuracy, the MEM technique was evaluated using realistic simulations. These simulations mimic interictal spikes propagating along the cortical surface.

Several studies in EEG and MEG demonstrated propagation patterns in epilepsy, notably in the temporal lobe [26, 5, 47] and the frontal lobe [26, 40]. Lantz et al. [56] indicated that the source localization was likely to be more accurate when analyzing the signal at around 50% of the rise time of the spike, since it is a tradeoff between the signal-to-noise ratio and the propagation of the source. Several authors considered MEG more efficient than EEG to identify the propagation pattern [85, 42], due mainly to the enhanced spatial resolution.

In this chapter, we first present the standard inverse solvers, using Tikhonov regularization (Section 3.2.1), before introducing the MEM framework, developed in our laboratory (Section 3.2.3). In Section 3.2.4, the process to simulate the interictal discharge is explained. The results for an example simulation and for a set of 100 simulations are shown in Section 3.3 and discussed in Section 3.4.

3.2 Materials and methods

In this section, the standard way of source localization, i.e. techniques using Tikhonov regularization, and the MEM techniques will be introduced.

3.2.1 Source localization using Tikhonov regularization

In the context of a distributed sources model, Dale and Sereno [21] proposed to constrain the generators to be located in the cortical surface with their orientation normal to the surface. The EEG/MEG inverse problem then becomes linear:

$$M = GJ + E \tag{3.1}$$

where M is a $n_s \times n_t$ matrix of the EEG or MEG data measured with n_s EEG or MEG sensors and n_t time samples. G is the $n_s \times n_d$ lead field matrix, i.e. the solution to the forward problem. G models the influence of each of the n_d dipolar generators distributed along the cortical surface on the n_s EEG or MEG sensors. J is the $n_d \times n_t$ matrix of the source distribution, characterizing the current density as a function of time on the cortical surface. The estimation of this matrix is the goal of the source localization. E is a $n_s \times n_t$ matrix that models the additive noise.

The number of sensors is usually around 64 for EEG and 275 for MEG. The number of dipoles taken into account was set a priori. It may vary between 1000 and 50,000. A low number of dipoles will lower the problem complexity, but reduce the spatial resolution. For this project, the number of dipoles n_d was about 4000.

One of the simplest ideas we can have to solve this problem is to use the least square estimate to find the J based on the data M and the forward solution G we modeled:

$$\hat{J}_{LS} = \arg\min_{J} \|M - GJ\|_F^2 \tag{3.2}$$

where $\|\cdot\|_F$ denotes the Frobenius norm. An analytical solution can be found using the differential of $\|M - GJ\|_F^2$. We obtain:

$$\hat{J}_{LS} = (G^T G)^{-1} G^T M \tag{3.3}$$

Unfortunately for our problem, this solution is not applicable: the number of sensors is always much lower than the number of dipolar sources distributed on the cortex ($n_s \ll n_d$), which makes G^TG impossible to invert. The Equation 3.1 is said to be ill-posed: a unique solution cannot be found without additional constraint or regularization. The Tikhonov regularization is one of the methods used to find a unique solution. With this method, the Equation 3.3 becomes:

$$\hat{J}_{MNE} = (G^TG + \lambda I)^{-1}G^TM \tag{3.4}$$

where I is the identity matrix, and λ is a hyperparameter to estimate. In the domain of EEG and MEG source localization, this method is called Minimum Norm Estimate (MNE), name given by Hämäläinen and colleagues [38]. The solution of this method provides the solution with the lowest energy in the source space:

$$\hat{J}_{MNE} = \arg\min_J \left(\|M - GJ\|_F^2 + \lambda \|J\|_F^2 \right) \tag{3.5}$$

λ is a hyperparameter controlling the proportion of regularity brought to the solution. It is related to the signal to noise ratio. The lower the level of noise, the lower the reconstruction error, and therefore the lower λ.

Different methods have been proposed to estimate λ. The method used for this study is called the L-curve method, and was first proposed by Hansen and colleagues [39]. The principle of this method is to calculate the inverse solution for

different values of λ. One can then represent on the same figure $\|M - GJ\|_F^2$ as a function of $\|J\|_F^2$ for different values of λ. The Figure 3–1 shows an example of this L-curve. The optimal λ is then selected as the point with the highest curvature, as shown in Figure 3–1 by the green lines. Indeed, when displaying the values of the residual norm ($\|M - GJ\|_F^2$) and the regularization term ($\|J\|_F^2$) for different values of λ, one can see a horizontal line and vertical line. The horizontal part (corresponding to high values of λ) shows oversmoothed solutions, only dominated by regularization errors. On the other hand, the vertical line, cases when λ is too small, show solutions dominated by perturbation errors. The L-Curve theory assumes the best solution lies in the corner of the two lines, assuring a tradeoff between the regularization and perturbation errors. The corner of the curve is found by selecting the point with the highest curvature.

We can generalize the minimum norm by changing the identity matrix in Equation 3.5 by a symmetric matrix K:

$$\hat{J} = \arg\min_J \left(\|M - GJ\|_F^2 + \lambda \|KJ\|_F^2 \right) \tag{3.6}$$

In that case, Equation 3.4 becomes:

$$\hat{J} = (G^T G + \lambda \Sigma_J)^{-1} G^T M \tag{3.7}$$

where $\Sigma_J = (K^T K)^{-1}$, a matrix related to the covariance matrix of the generators. The assumptions put on the solution of your source localization depend of the nature of K:

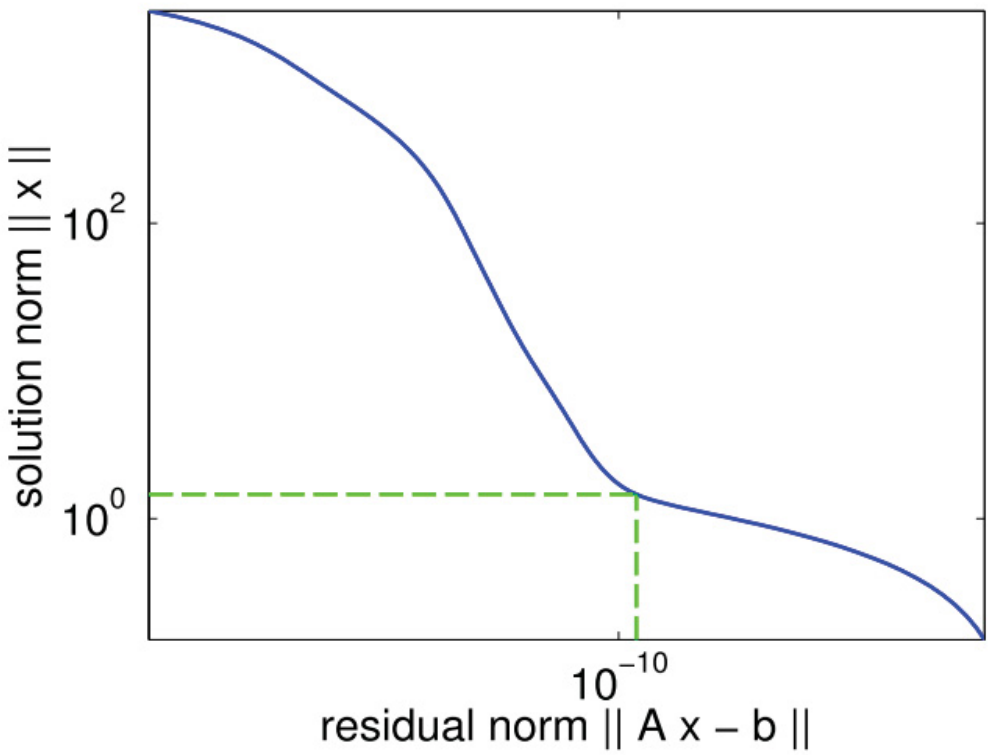

Figure 3–1 – L-curve in minimum-norm estimator. The curve is displayed in a *log-log* scale. Taken from [34]

- If $K = I$, as for the **minimum norm** method, it means that the generators on the cortex are considered as independent and contributed identically to the data
- If $K = W$, with W being a diagonal matrix, the method is called **weighted minimum norm**. It is based on the fact that all the generators do not contribute similarly to the data. Indeed, superficial sources have a higher effect on the data than deep sources. Therefore, using a minimum norm method penalizes deep sources over superficial ones. W is then used to

cope with this bias. Generally, we set the diagonal elements of W as $w_i = \|G_i\|^\gamma$, with $\gamma = 1$ or 2, where G_i is the ith column of the gain matrix G. The difference of norm of the columns of the gain matrix is therefore counterbalanced by the W matrix. That way, all the generators have the same impact on the data.

– If K is a spatial Laplacian matrix, the solution is the one with the highest spatial smoothness. The formulation is similar to the method called LORETA, developed by Pascual-Marqui et al. [77].

3.2.2 Connection with the Bayesian framework formulation

Within the Bayesian framework, given Equation 3.1 we consider that E and J are Gaussian distributions with null mean and of variance of $\sigma_E^2 I_n$ and $\sigma_J^2 (K^T K)^{-1}$ respectively. The inverse problem can be viewed as the conditional probability of J given the data M. According to Bayes' law:

$$p(J|M) = \frac{p(M|J)p(J)}{p(M)} \tag{3.8}$$

where $p(M|J)$ is the data likelihood, and $p(J)$ is the prior distribution representing the information brought by J.

Within this Bayesian framework, a solution to this inverse problem can be found by using the Maximum a Posteriori estimate of J, which is equivalent to maximizing the log-posterior probability:

$$\hat{J}_{MAP} = \arg\max_J p(J|M) = \arg\max_J p(M|J)p(J) = \arg\max_J \left(\ln p(M|J) + \ln p(J)\right) \tag{3.9}$$

Given the distribution of E and J, the equation becomes:

$$\hat{J}_{MAP} = \arg\min_{J} \left[\|M - GJ\|^2 + \lambda \|KJ\|^2 \right] \tag{3.10}$$

where $\lambda = \frac{\sigma_E^2}{\sigma_J^2}$.

Hence, the solution is then given by:

$$\hat{J}_{MAP} = \left(G^T G + \lambda (K^T K)^{-1} \right)^{-1} G^T M \tag{3.11}$$

which is equivalent to Equation 3.7

3.2.3 Source localization within the MEM framework

MEM principle

The MEM approach considers J as a realization of a multivariate random variable with a probability distribution $dp(j) = Prob(J = j)$. Regularization is introduced by writing the solution in the form of $dp(j) = f(j)d\mu(j)$ where the reference distribution $d\mu$ models the a priori information and f is a μ-density to be found such that dp can explain the data on average:

$$M = \int jGf(j)d\mu(j) \tag{3.12}$$

Figure 3–2 illustrates the principle of the MEM. Let us define C_m as the set of the distributions solving Equation 3.12 and μ is the reference distribution. The MEM solution is the solution $\tilde{p}$ which minimizes the mu-entropy of dp, $S_\mu(p)$, which is nothing else than the opposite of the Kullback-Leibler divergence between p and μ. Let us define as p^* the 'true solution' and belongs to C_m. One can see

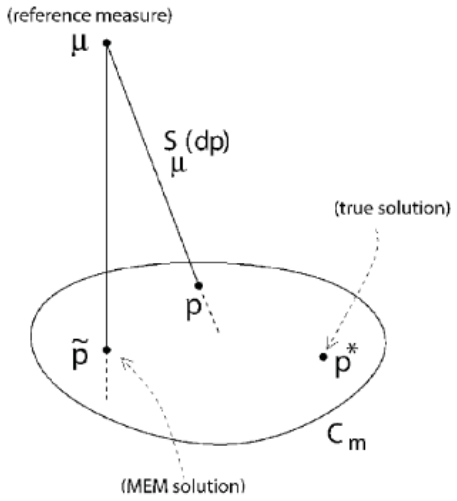

Figure 3–2 – Illustration of MEM : C_m is the set of the solutions. $\tilde{p}$ is the MEM solution, which is the 'closest' density to the prior μ. Taken from [2].

that the relevance of the solution, i.e. the distance between $\tilde{p}$ and p^*, depends almost entirely on the relevance of the reference $d\mu$. It is thus very important to define an appropriate reference distribution.

Initialization of the reference distribution

To define the reference distribution, the MEM model originally proposed by Amblard et al [2] and used in this thesis uses cortical parcels, in which all the generators are spatially connected. Thus, initializing the reference distribution $d\mu$ will first consist in decomposing the whole cortical surface into n_k non-overlapping parcels . This allows to impose a different prior for each parcel, instead of considering all the dipoles individually. To do so, we proposed a spatial clustering based on a data-driven parcelization (DDP) method [23, 57]. This method is based on the multivariate source prelocalization (MSP) method [61]. The MSP provides for each dipole an index corresponding to the probability of this

dipolar generator to contribute to the solution. The seed points for each parcel are found among the local maxima of the MSP coefficients, and neighboring dipoles will gather the parcel at the condition they contribute to the same underlying generator. For detailed information, refer to Chowdhury, 2011 [15]. A cortex composed of around 4000 generators is clusterized in sets of between 35 to 150 parcels.

Each parcel k is characterized by a hidden activation state S_k, describing if the parcel is active ($S_k = 1$) or not ($S_k = 0$). If the parcel is active, the intensity of the generators within the parcel is assumed to follow a Gaussian distribution. On the other hand, generators belonging to an inactive parcel are assumed to follow a Dirac delta distribution, meaning that the parcel is "shut down" (the current density of all the generators is set to 0) and does not contribute to the data. If α_k is the probability for the parcel k to be active: $\alpha_k = p(S_k = 1)$. Information about distributions can be found in Everitt et al., 2010 [28]. The reference distribution of the kth parcel is:

$$d\mu_k(j) = (1 - \alpha_k)\delta(j_k) + \alpha_k \mathcal{N}(\mu_k, \Sigma_k)(j_k) \tag{3.13}$$

Assuming the K parcels to be mutually independent, prior information for the MEM was introduced by the reference distribution $d\mu$ defined by the following product of mixtures:

$$d\mu(j) = \prod_{k=1}^{n_k} d\mu_k(j) = \prod_{k=1}^{n_k} \left[(1 - \alpha_k)\delta(j_k) + \alpha_k \mathcal{N}(\mu_k, \Sigma_k)(j_k)\right] dj \tag{3.14}$$

For each parcel, α_k were initialized using the median of MSP score of the generators within the parcel k. μ_k was set to zero. For MEM, Σ_k was a diagonal matrix, whose diagonal was calculated using 5% of the mean of the square of the activity on the parcel provided by MNE localization. The same process was used for cMEM to calculate Σ_k except that it was afterward multiplied by a Green's function of the adjacency matrix, in order to impose spatial smoothness within the parcels [16].

MEM resolution

The μ-entropy of the distribution dp is then given by:

$$S_\mu(dp) = -\int dp \log \frac{dp}{d\mu} = -\int f(j) \log f(j) d\mu \tag{3.15}$$

The MEM solution is found by maximizing $S_\mu(dp)$ with respect to the data.

$$\begin{cases} J_{\text{MEM}} = \int j \ \widehat{dp} \\ \widehat{dp} = \arg\max_{dp} S_\mu(dp), \text{ with } \int dp = 1 \text{ and } M - G \int j \ dp = 0 \end{cases} \tag{3.16}$$

This equation can be solved using the Lagrange method. The Lagrange function to minimize is:

$$L(dp, a, b) = -S_\mu(dp) + a(1 - \int dp) + b\left(M - G \int j dp\right) \tag{3.17}$$

where a and b are Lagrange parameters.

The MEM solution is then given by:

$$\widehat{dp} = \frac{e^{\hat{b}^T G j}}{\int e^{\hat{b}^T G} d\mu} d\mu \tag{3.18}$$

where $\hat{b}$ is the maximum of the optimization function $D(b)$:

$$\hat{b} = \arg\max_b D(b), \text{ where } D(b) = b^T M - \log \int e^{\hat{b}^T G d\mu} d\mu - \frac{\Sigma_E}{2} b^T b \tag{3.19}$$

where Σ_E is the covariance matrix of the noise E in Equation 3.1.

The maximization of $D(b)$ is done iteratively until convergence using an unconstrained nonlinear optimization (using Matlab optimization toolbox). It can be shown that $D(b)$ is a convex function, meaning that there are no local maxima. Moreover, the dimension of that function is the number of sensors and not the number of generators. Therefore, the complexity of the optimization problem does not depend on the precision of the cortical surface (i.e. the number of vertices).

Given the Equations 3.14 and 3.18, we can note that the solution for each parcel k is given by:

$$J^k_{\text{MEM}} = \hat{\alpha_k} \left(\mu_k + \Sigma_k G_k^T \hat{b} \right) = \hat{\alpha_k} \Sigma_k G_k^T \hat{b} \tag{3.20}$$

$\hat{\alpha_k}$ is found based on $\alpha_{k,\text{init}}$:

$$\hat{\alpha_k} = \frac{\alpha_{k,\text{init}}}{\alpha_{k,\text{init}} + (1 - \alpha_{k,\text{init}})e^{-\frac{1}{2}{b^n}^T G_k \Sigma_k {G_k}^T b_n}} \tag{3.21}$$

G_k is the submatrix of G containing the columns of the generators present in parcel k.

3.2.4 Simulation of propagating interictal spikes

Modeling an interictal spike

Simulations containing simulated interictal spikes were created. The simulated signal lasts few milliseconds and contains a spike propagation along the cortical surface, the whole being contaminated by realistic additive noise. For the matter of statistics, a 100 of this kind of events were simulated. The different source localization methods were then applied on the simulated data. As the ground truth was fully controlled, validation metrics could be developed to assess the performance of each method.

The construction of the simulation consisted of three main steps. First, the theoretical data are simulated. This corresponds to the gold standard: it consists in modeling the spatio-temporal patterns (location, duration, propagation, amplitude) of the active dipoles mimicking the generators of epileptic activity. Then, the forward problem is applied to the theoretical current density distribution in order to simulate corresponding activity on the sensors. Then simulated data are corrupted using realistic noise that consists in real EEG/MEG background.

EEG/MEG background activity was taken from a patient with focal epilepsy for whom no epileptic brain activity could have been identified. Informed consent for the study was obtained as approved by the research ethics committee of the Montreal neurological institute and hospital. A high resolution T1 weighted MRI was acquired on the patient at the Montreal neurological institute. In order to estimate the cortical surface of the patient, we used a segmentation of the white/gray matter interface, computed with BrainVISA software ([32] - `http://www.brainvisa.info`). The solution of the forward problem was computed using a 1-layer boundary element method (BEM) model [54] using OpenMEEG software ([35, 55] - `http://www-sop.inria.fr/odyssee/software/OpenMEEG/`). BEM was performed using the inner surface of the skull. MEG data were obtained at the MEG center of université de Montréal on a 275-channel CTF whole-head MEG system. The relative position of the sensors from the head was tracked with localization coils placed on three fiducial points. Coregistration between the sensors positions and the MRI data was done with a manual localization of the fiducial points of the MRI images.

A source of epileptic spike was modeled as a region of activation randomly located on the cortical surface. A source corresponds to an extended region of activity. It is characterized by a seed point, i.e. the center of the source, and a spatial extent. The seed point is chosen randomly among the vertices of the cortical mesh. The spatial extent is expressed by a degree of spatial neighborhood around the seed point. If the spatial extent is one, the source will be composed by the seed point, and the vertices directly next to it, i.e. the nodes of the cortical

mesh connected to it. If the spatial extent is two, the source will contain the seed point, its neighbors, and the neighbors of its neighbors along the cortical surface; and so on. For each dipolar source of the simulated spatially extended generator, the same time course and amplitude was applied, even though such an assumption is not realistic. The time course of an interictal spike was modeled as the sum of 3 gamma functions (see Figure 3–3). It consists in a spike lasting about 250 ms and a positive and a negative peak, followed by a slow wave, which is a typical interictal pattern [69].

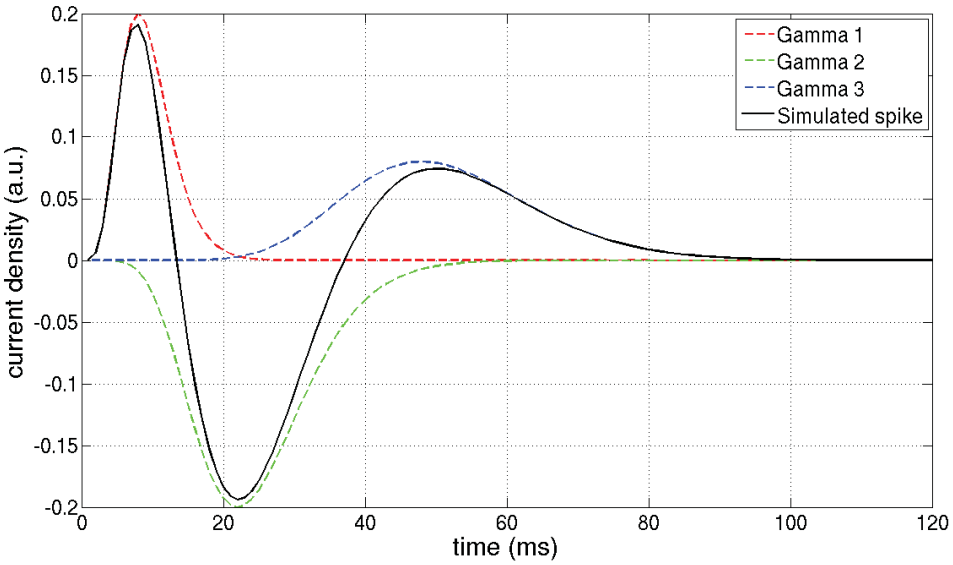

Figure 3–3 – Simulated interictal spike.

With the spatial extent of the sources and their time course, it is possible to create the matrix J_{th}, corresponding to the 'ground truth', the gold standard that will be used for evaluation of the source localization methods. Then, for each

dipole belonging to a source, the corresponding row of J_{th} is the time source of the source. All the dipoles not involved in any epileptic source were set to 0.

Propagation pattern

To simulate the propagation of the spike, we proposed to start by simulating a simple but realistic pattern of propagation, which mimics the activity between two cortical sources linked by axonal transmission. It simulates a spike which onsets at a specific location of the brain and propagates on a region connected to the irritative zone. An example of this propagation is illustrated in Figure 3–4.

For these simulations, the sources of onset and propagation are randomly chosen on the surface of the cortex. The time course of the two sources are identical, the region of propagation is simply activated few milliseconds after the onset of the spike. The delay of propagation depends on the distance between the two regions, with a speed of propagation to 1 m/s [26]. This type of propagation is realistic in epilepsy and concordant with the literature [5, 47], and can express a remote activation of a neural network connected to an active population by a fiber track.

Realistic noise

In realistic data the signal to noise ratio (SNR) depends on the depth of the sources. To mimic this property, the simulated source distribution was normalized so that the maximum amplitude that could be seen on the MEG data was 1.5 pT, the expected order of magnitude for a spike [1]:

$$J_{th}^{n} = J_{th} \times \frac{1.5}{\max(|G|)} \tag{3.22}$$

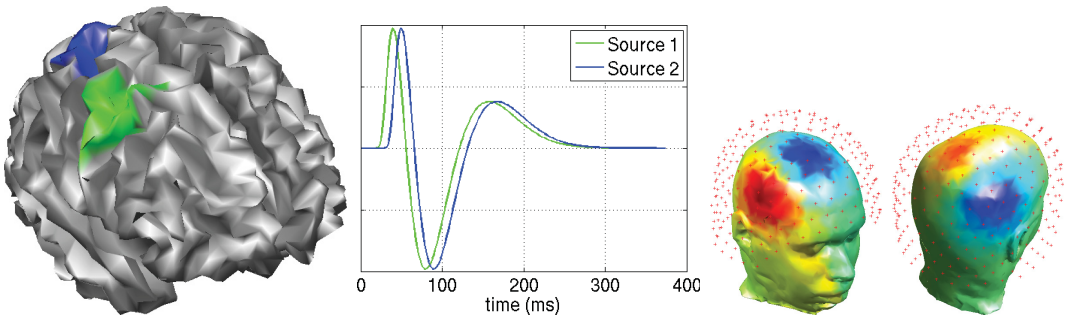

Figure 3–4 – Illustration of a propagation on a source going from the right central lobe to the right superior parietal lobe. **Left:** Spatial distribution of the source onset zone (green) and the propagation zone (blue). **Middle:** time courses of activation of the two regions. The delay between the two region is set to 12ms. **Right:** Topographic maps at the peak of activity for the source onset zone (t = 38ms) and the propagation zone (t = 50ms). The red dots represent the MEG sensors. The signal is projected on the skin of the subject: the red color represents a measured magnetic field going out of the head and the blue color the field going inside the head.

In order to corrupt our simulated data using realistic noise, we decided to use noise taken from a set of real MEG data containing no traces of epileptic activity. Several 700-ms segments of MEG data were prepared and stored. The noise was then randomly chosen among the segments of background activity. It was added according to the SNR:

$$signal = \text{SNR} \times signal_{\text{no noise}} + \text{noise} \tag{3.23}$$

where $signal_{\text{no noise}} = GJ^n_{th}$. The source localization methods were then applied to the noisy simulated signals. Each of them will calculate an inverse solution $\hat{J}$.

The validation metrics will then evaluate the quality of the results to compare the methods.

Following this simulation strategy, MEG signals generated by deeper sources will be of smaller amplitudes than the superficial ones. Consequently, the SNR for deep sources will be lower, which is consistent with real epileptic activities.

3.2.5 Validation metrics

This section presents all validation metrics we proposed to assess the performance of the three methods (MNE, MEM and cMEM) when applied to the simulated MEG data previously described. Each metric compared the source localization result to the ground truth. The proposed metrics focused on two aspects of the accuracy of the reconstruction: the ability to localize and to estimate the spatial extent of a source without spurious activity, and the accuracy of the reconstruction of source time courses.

I proposed four metrics to validate the spatial accuracy of source localization results: the RMS error calculated the sensitivity of the reconstruction, i.e. the accuracy of the reconstruction of the source, whereas E_{close} and SA quantified the specificity, in other words the amount of spurious activity. The metric E_{close} was proposed to assess the false positive which is close to the simulated source, whereas the metric SA was proposed to detect distant falsely activated sources. The area under the ROC curve (AUC) provides a score based on both sensitivity and specificity.

The shape error (SE) quantifies the accuracy of the temporal reconstruction of the source localization. Details of the five metrics are given below.

Notations

Let $J_{th} = J_{th}(\theta, t)$ be the theoretical current density, and $\hat{J} = \hat{J}(\theta, t)$ its estimation, θ being the source index. t denotes the time parameter, and n_t is the length of the time series. The superscript $\{\ ^n\ \}$ denotes the normalization of the matrix over time and space: for example, $\hat{J}^n = \frac{\hat{J}}{\max(|\hat{J}(\theta,t)|)}$.

Θ represents the set of all the dipoles of the cortical mesh, and Θ_{a_1} and Θ_{a_2} the set of dipoles belonging respectively to the two simulated sources. $\Theta^j(a_i)$ represents the set of vertices located within a local spatial neighborhood of degree j or less around the region Θ_{a_i} ($i = 1$ or 2). *card* represents the number of elements (vertices) of a set and the operator $\setminus$ is used for the set-theoretic difference.

Root mean square (RMS) error

To represent the goodness of fit, we used the root mean square of the error of the mean of $\hat{J}$ in the zone of activity:

$$RMS(a_i) = RMS\left(m_{a_i}(J^n_{th}) - m_{a_i}(\hat{J}^n)\right) = \sqrt{\frac{\sum_t^{n_t}\left(m_{a_i}(J^n_{th}) - m_{a_i}(\hat{J}^n)\right)^2}{n_t}} \quad (3.24)$$

with $m_{a_i}(J) = \sum_{\theta\in\Theta_{a_i}} \frac{J}{p_{a_j}}$ and $p_{a_i} = card(\Theta_{a_i})$.

The lower this criterion, the better the estimation fits with the theoretical data in amplitude and in shape in the region of interest.

Energy within a close neighborhood of the source ($\mathbf{E_{close}}$)

In order to look at the amount of false positive due to an overestimation of the spatial extent or a small error in location around the main generator, we considered the energy of the mean of the activity in a close neighborhood around the source, but excluding the source. It was then normalized by the energy of the theoretical time course.

$$E_{close}(a_i) = \frac{\sum_t^{n_t} \left(\sum_{\theta \in \Theta^3(\Theta_{a_i}) \setminus \Theta_{a_i}} \frac{|\hat{J}|}{p} \right)^2}{\sum_t^{n_t} \left(\sum_{\theta \in \Theta_{a_i}} \frac{|\hat{J}|}{card(\Theta_{a_i})} \right)^2} \tag{3.25}$$

with $p = card(\Theta^3(\Theta_{a_i}) \setminus \Theta_{a_i})$

A high value of $\hat{E}_{close}$ means either the estimation misplaced the center of activity, or the spatial extent of the source was larger than expected.

Spurious activity (SA)

Source localization techniques sometimes find activity far from the actual source of activity (e.g. on the contralateral side). Those results may be very misleading. SA indicator was calculated by counting the number of dipoles located far from the actual sources, reaching a certain threshold τ. This threshold was set as 30% of the maximum of amplitude at the peak of the signal. The dipoles taken into account were those having more than two degrees of neighborhood of distance from an active region. This index is a percentage showing the amount of active dipoles among all the vertices far from the sources.

$$SA = \frac{card(\Omega)}{card(\ \Theta \setminus (\ \Theta^3(\Theta_{a_1}) \cup \Theta^3(\Theta_{a_2})\ )\ )} \tag{3.26}$$

where $\Omega = \left\{ \theta \mid \theta \in \Theta \setminus \left(\Theta^3(\Theta_{a_1}) \cup \Theta^3(\Theta_{a_2})\right), \exists t \, |\hat{J}|^n(\theta, t) > \tau \right\}$

Shape error (SE)

This indicator was used to show the accuracy of the temporal reconstruction inside an activated region. This metric was calculated for each source of the simulation.

SE was obtained by taking the mean of the time courses of the dipoles of the reconstructed source. The time vector was then normalized, so that its values are between -1 and 1, and compared to the simulated time source. SE was then the root-mean square (RMS) of the error between the gold standard and the reconstructed data. Therefore, the smaller SE, the better the source reconstruction in the region of interest. The aim of this metric was to focus on the error on the shape of the time course.

$$SE(a_i) = \sqrt{\frac{\sum_t^{n_t} \left(\frac{m_{a_i}(J_{th})}{\max(|m_{a_i}(J_{th})|)} - \frac{m_{a_i}(\hat{J})}{\max(|m_{a_i}(\hat{J})|)} \right)^2}{n_t}} \tag{3.27}$$

Area under the Curve (AUC)

This metric was proposed in Grova et al., 2006 [36] and Chowdhury, 2011 [15] for evaluation of static simulation on EEG and MEG in order to assess the ability of source localization method to recover the source and its spatial extension at the

main peak of the simulated signals. It is based on receiver operating characteristic (ROC) curves [63]. This criterion does not use the temporal dimension: the AUC is calculated only at the peak of the spike.

The criterion looks at the normalized energy of each source at a specific time sample. For a threshold τ ($0 < \tau < 1$, 1 being the maximum of amplitude), a dipolar generator is considered to be active if the amplitude of the generator is larger than τ. By comparing the set of estimated active sources to the Gold Standard, it is possible to quantify the amount of true positive (TP), true negative (TN), false positive (FP) and false negative (FN). The ROC curve is then obtained by selecting different values of τ between 0 and 1 and representing the sensitivity ($\frac{TP}{TP+FN}$) against (1 - specificity ($\frac{TN}{TN+FP}$)). The AUC is a metric quantifying the area under this curve, i.e. AUC$= \sum_\tau \frac{y(\tau)+y(\tau+1)}{2}(x(\tau+1)+x(\tau))$ with x and y respectively the abscissa and ordinate of the curve.

AUC is often seen as the probability that the amplitude of an active source is greater than an inactive one. In practice, a detection method showing an AUC index greater than 0.8 is generally considered as sufficiently accurate [36], allowing 80% of good detections.

For a better estimation of the AUC, it is preferable to have the same number of activated and non-activated generators for the construction of the ROC curve. In our case, there are many more inactive sources than active ones. Therefore the specificity may be biased: it tends to be artificially high. For that reason, few changes were proposed to the unbiased calculation of the AUC. We separate the generators which are located near the source of activation, and the ones which are

distant from it. The value of the AUC is the arithmetic mean between two values: $\mathrm{AUC}_{\mathrm{close}}$ and $\mathrm{AUC}_{\mathrm{far}}$.

- We considered as "close" all the dipolar generators located within the 10th neighborhood order around the simulated source. If d_a generators were contributing to the simulated source, d_a inactive generators were randomly selected among all the closed generators.
- $\mathrm{AUC}_{\mathrm{far}}$, considered all the generators that are not close to the source. As for $\mathrm{AUC}_{\mathrm{close}}$, we picked the same number of generators which were non-activated as the ones contributing to the source. To prevent from picking generators from the same regions, we used the clusters to select the generators that was used for the computation of the ROC curve. To do that, we selected the generators which were the most active for each cluster, then the second most active, and so on until the number of selected generators equals the number of generators in the source. This selection of the local maxima located far from the source was used for $\mathrm{AUC}_{\mathrm{far}}$ to be sensitive to eventual spurious activity,

To obtain a robust metric, we calculated $\mathrm{AUC}_{\mathrm{close}}$ and $\mathrm{AUC}_{\mathrm{far}}$ $N = 30$ times and computed the mean of all the iterations. Concretely, we have:

$$AUC = \frac{1}{2}\sum_{i=1}^{N}\frac{\mathrm{AUC}_{\mathrm{close}}^{i}}{N} + \frac{1}{2}\sum_{j=1}^{N}\frac{\mathrm{AUC}_{\mathrm{far}}^{j}}{N} \tag{3.28}$$

where $\mathrm{AUC}_{\mathrm{close}}^{i}$ and $\mathrm{AUC}_{\mathrm{far}}^{j}$ is respectively the ith and jth iteration of $\mathrm{AUC}_{\mathrm{close}}$ and $\mathrm{AUC}_{\mathrm{far}}$.

Simulations were performed for 100 pairs of sources located randomly on the cortical surface. Noise was added on the simulated sources with a SNR of 3. 20 simulations of the same source were computed, and averaged. MNE, MEM and cMEM source localization were performed. For the propagation pattern, the distance between the two sources was 10 degrees of spatial neighborhood (mean geodesic distance : 73mm).

3.3 Results

Illustration on one simulated data set

This section presents the results of a simulation of a source propagating from the left superior parietal lobe to the left angular gyrus. Both sources are superficial (eccentricity $>$ 70mm, where the eccentricity is defined as mean distance between the source and the centre of the cortical surface [1]). We therefore expect such a source reconstruction to be accurate, since superficial sources are easier to be detected [4]. Figure 3–7(a)(e) shows the spatial distribution of the simulated sources.

Figure 3–5 represents the MEG channel overlay, and two markers were added to show the time of the peak of the two sources. Figure 3–6 shows the topographic maps, i.e. the projection of the sensors data on the skin of the patient at the peaks. The signal topography clearly exhibits a dipolar pattern at the peak of the first source, that is to say a negative and a positive component.

1. The centre of the cortical surface is defined with the fiducial points. It is the point which is equidistant to the left and right periauricular points, at the same height of the location of the nasion.

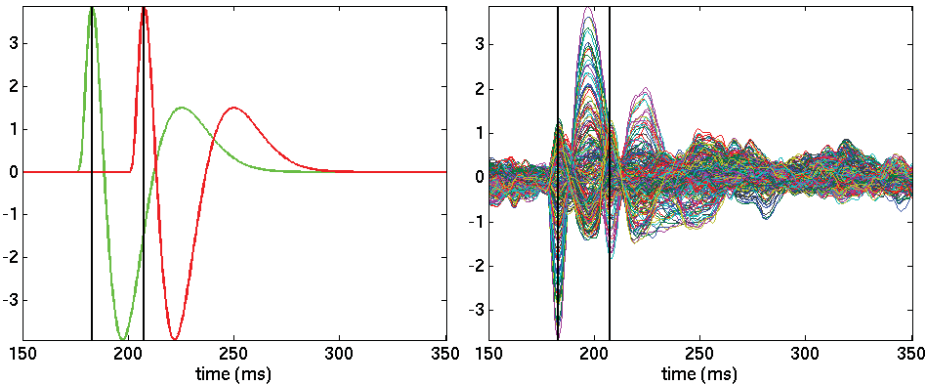

Figure 3–5 – Sources time courses (**left**) and MEG channel overlay plot of the simulated signal (**right**). The vertical bars represent the time event of the positive peak of source 1 and 2.

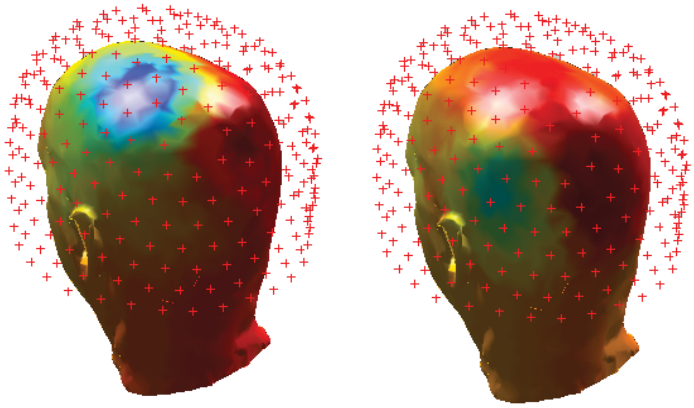

(a) Signal 1 (b) Signal 2

Figure 3–6 – Topographic maps of the simulated MEG signal shown in Figure 3–5 during the peaks of activity.

Source localization results obtained using MNE, MEM and cMEM are presented in Figures 3–7(b)(f), 3–7(c)(g) and 3–7(d)(h) respectively. All these results are presented as the absolute value of the current density at the peak of each of the two simulated spikes, and thresholded using Otsu threshold, which finds a threshold minimizing the inter-class variance [73]. The figures show that

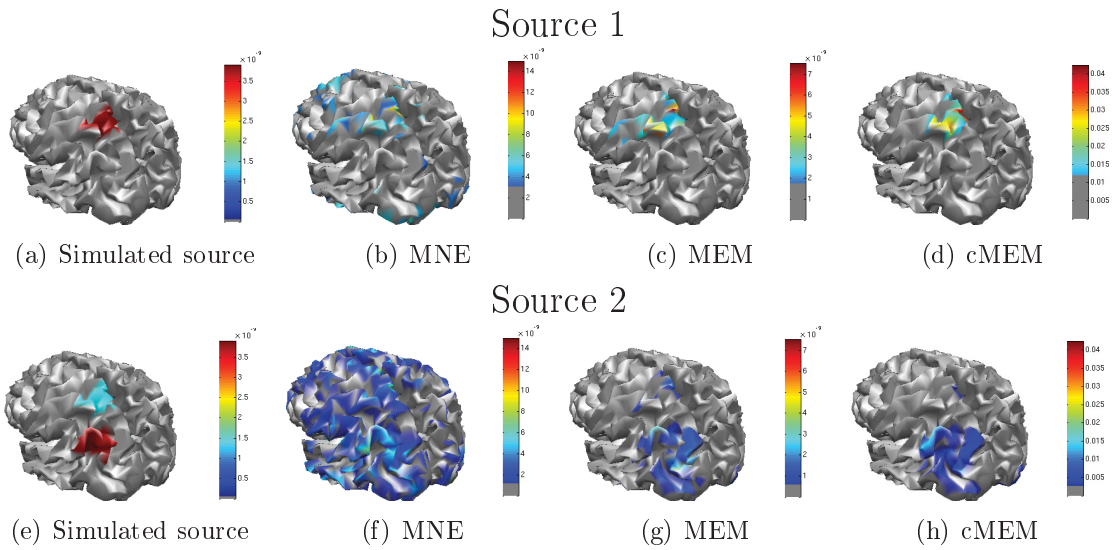

(a) Simulated source (b) MNE (c) MEM (d) cMEM

(e) Simulated source (f) MNE (g) MEM (h) cMEM

Figure 3–7 – Spatial distribution of a simulated source and its reconstruction using MNE, MEM and cMEM. The absolute value of the amplitude of the dipoles is represented here. The colors indicate the level of amplitude, from blue, which represents low amplitude to dark red, the maximum of amplitude. All the maps are thresholded using Otsu threshold at both peak.

MEM and cMEM source reconstructions at the first peak of the spikes have a similar spatial extent to the simulated source. For the second source however, all techniques failed to correctly estimate the spatial extent.

All the results of the metrics estimated on the source localization results are presented in Figure 3–7 and in Table 3–1.

SA metric, reflecting the amount of false negative in remote regions, shows that MEM amd cMEM did not reconstruct any spurious activity. This false positive rate reaches 7% for MNE.

Table 3–1 – Results of the metrics of the simulation shown in Figures 3–7 and 3–5. In bold are the best results (maximum or minimum, depending on the metric) for each source.

Metrics	*MNE*		*MEM*		*cMEM*	
	Source 1	Source 2	Source 1	Source 2	Source 1	Source 2
SA	0.07		**0.00**		**0.00**	
AUC	0.76	0.73	0.92	0.74	**0.97**	**0.92**
RMS error	**0.87**	**1.87**	1.24	2.26	1.94	2.59
SE	**0.11**	**0.08**	0.14	0.28	0.25	0.27
E_{close}	1.66	3.86	1.83	1.71	**1.01**	**0.20**

As one can notice visually in Figure 3–7, the MNE solution is not sensitive to the spatial extent, when compared to MEM and cMEM. This would be reflected by the AUC scores at the time of the peaks.

The computation of the RMS error is illustrated in Figure 3–8. It shows the mean time course of reconstructed amplitude within the simulated source and compares it with the theoretical simulated time course. The metric then consisted in the RMS errors between these two curves. For both sources, the error was lower for MNE, as MEM and cMEM tended to underestimate the amplitude of the source.

SE qualifies the ability for the methods to accurately reconstruct the shape of the simulated time course, while normalizing the amplitude. SE results are presented in Table 3–1 and in Figure 3–9. One can see that for this example, MNE provided a better score than MEM and cMEM.

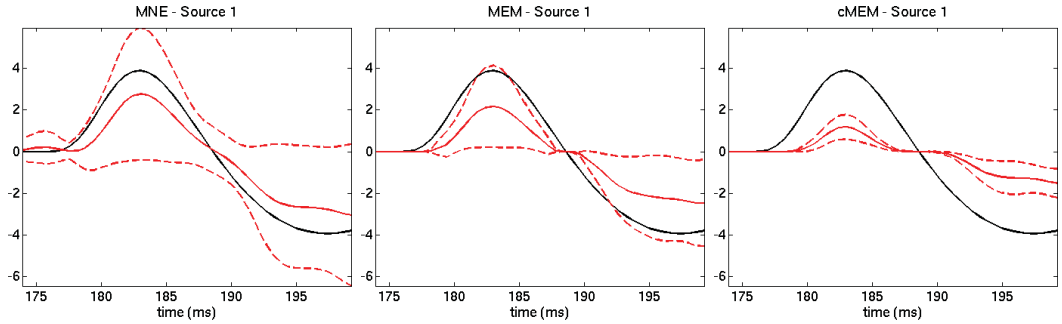

(a) Source 1

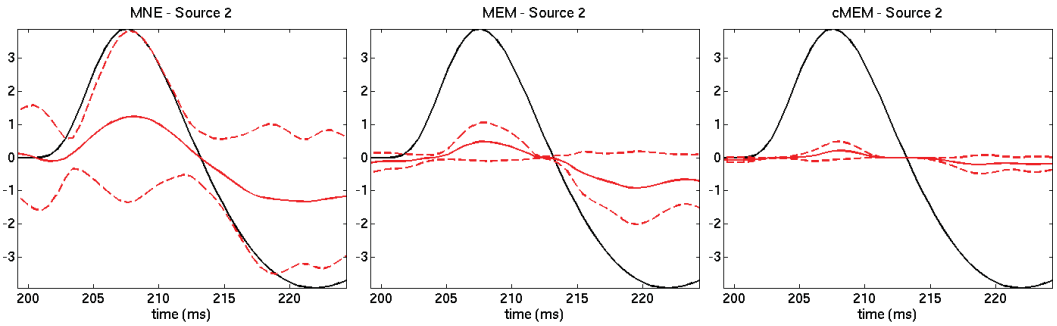

(b) Source 2

Figure 3–8 – Mean of the reconstructed time courses of the dipoles located within the simulated source in Figure 3–7 (in red). The dashed lines are the standard deviation values. In black is drawn the simulated time course of the source. The RMS of the difference between the two curves give the RMS error of the source.

E_{close}, as shown in Figure 3–10, reveals that cMEM was the method with the least energy near the sources, meaning that this method showed no spurious activity near the source.

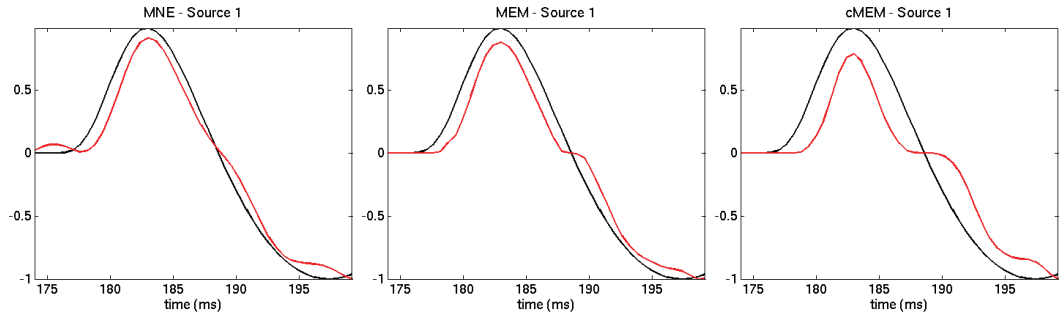

(a) Source 1

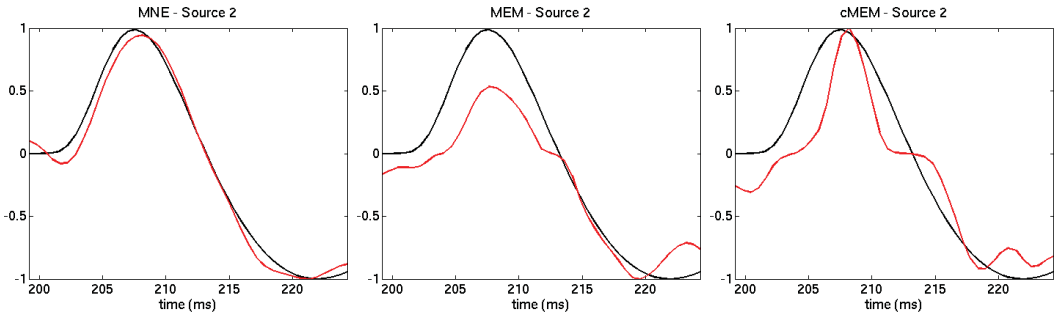

(b) Source 2

Figure 3–9 – Mean of the reconstructed normalized time courses of the dipole located in the simulated source in Figure 3–7 (in red). In black is drawn the simulated time course of the source. The RMS between these two curves is the SE metric.

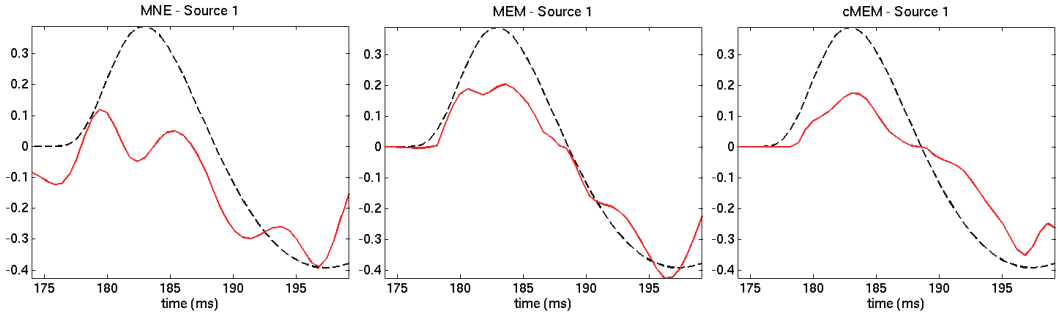

(a) Source 1

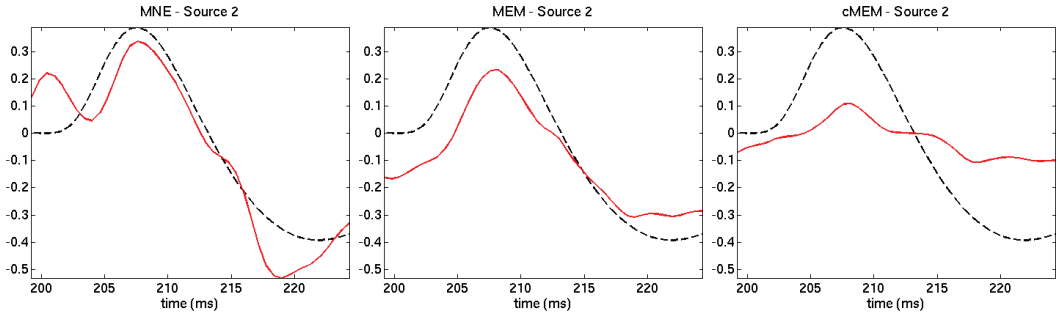

(b) Source 2

Figure 3–10 – Result of the energy in the region close to the source (in red). The dashed black line corresponds to the 10% amplitude of the theoretical source time course, for the matter of comparison.

Result for 100 simulations

Distribution of AUC scores over the 100 simulations is represented using boxplot in Figure 3–11(a). The AUC score for MEM techniques was higher than the MNE. The median of the AUC for the MEM techniques for each source was above 0.8, meaning that most of the reconstructions presented excellent results. The source 2 had most of the time a lower AUC than source 1, which was due to the fact that the first source was affecting the localization of source 2. With the two sources to localize at the same time, even if the generators of the first source were not considered for the computation of the AUC of source 2, the SNR at the peak of the second source was obviously lower because of the temporal overlap between the simulated time courses of the two sources as shown in Figure 3–11(a).

Figure 3–11(b) presents the boxplot distribution of RMS error values for each method over the 100 simulations. We observed that the lower RMS error values were obtained for MNE, followed by MEM and then cMEM.

Boxplot distributions of E_{close} and SA value are presented in Figures 3–11(c) and 3–11(d). Concerning E_{close}, the results were similar for MNE and MEM, and lower for cMEM. The median of spurious activity found with SA reached 6% for MNE, whereas it was only around 1% for MEM and cMEM.

The temporal accuracy of the reconstruction, represented by SE, is shown in Figure 3–11(e). Globally, MNE and MEM performed similarly in term of SE score. cMEM, on the other hand, obtained higher values, meaning that the temporal accuracy of this method was lower.

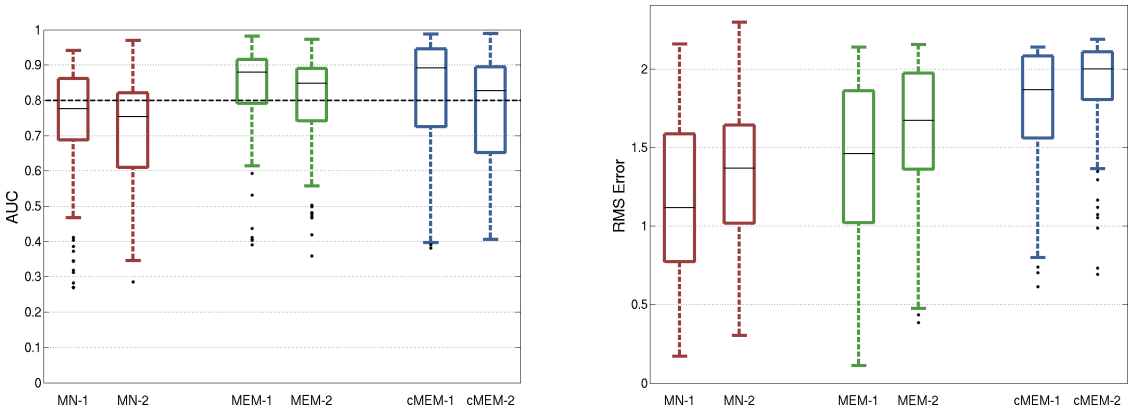

(a) AUC

(b) RMS error

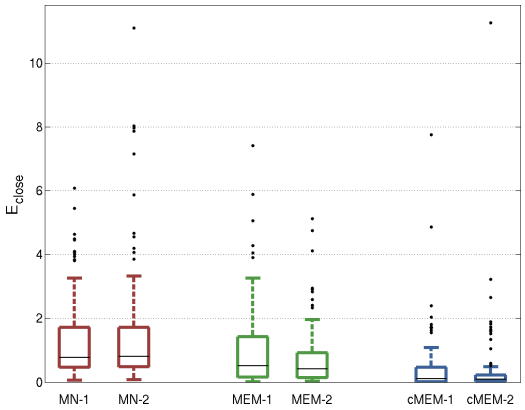

(c) E_{close}

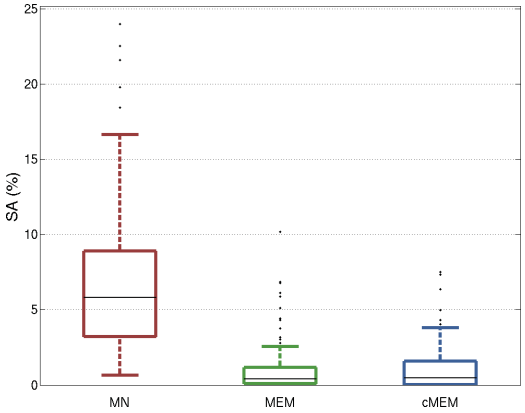

(d) SA

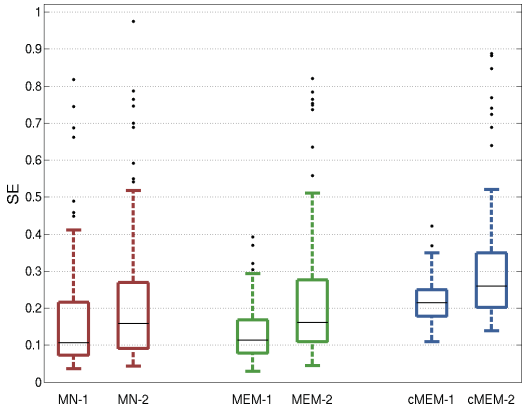

(e) SE

Figure 3–11 – Distribution of the validation metrics (AUC,RMS error,E_{close},SA,SE) obtained over the 100 simulations, using boxplot representations. The black points represent the outliers. For AUC, the points above the dashed line (0.8) are considered good detection.

3.4 Discussion

The purpose of the project was to simulate spatio-temporal MEG signal containing the propagation of an interictal spike and to evaluate the performance of different source localization methods.

We simulated a signal composed of two distinct sources, where a spike (modeled by 3 gamma functions) propagated from one to another region, after a certain delay. Several assumptions were made, such as the population being composed of a set of equivalent dipoles which were represented by the nodes of a cortical mesh. Moreover the two sources were imposed to be in the same hemisphere, whereas other studies were referring to propagation to the contralateral hemisphere [26].

Besides, the simulated signal was made by averaging 20 trials of the same propagation pattern. This assumes that it is possible to record signals which have exactly the same origin and spatial extent, and propagate exactly the same way. This is obviously physiologically incorrect. Further studies will correct this error by using single trial data for source localization. Moreover, it would be interested to work with more accurate models of interictal spikes and propagation patterns. Cosandier-Rimélé et al [19] for instance developed a model of neuron populations able to generate realistic intracranial and scalp EEG especially in epilepsy.

During this study, we aimed at quantifying the ability of three distributed source localization methods to reconstruct this spatio-temporal signal. We used to validate the results the Area under the ROC curve [36] as well as other validation

metrics specifically proposed for the present study to test the accuracy in space (RMS error, E_{close}, SA) and in time (SE).

For spatial accuracy, our results using AUC on simulations involving two generators were in agreement with our previous findings [16], i.e. MEM and cMEM demonstrated better performances than MNE. Our results showed that the MEM source localization was able to accurately reconstruct the epileptic source even in the context of a propagating source. Indeed, whereas the localization of source 1 corresponded to scenarios investigated in previous studies, at the peak of source 2, the data was still contaminated by source 1, reducing the signal to noise ratio.

In term of sensitivity of the simulated source, MNE obtained a lower RMS error than the other techniques. One of the reasons explaining this finding is that MEM techniques tend to underestimate the amplitude of the current, which increases the RMS error.

On the other hand, the MEM methods clearly showed better spatial specificity than MNE. The ability for the MEM techniques to shut down cortical parcels clearly reduced the number of spurious sources, as demonstrated by SA. Moreover, the spatial extent of the source was better estimated with the entropic techniques, as demonstrated by E_{close}.

The ability to reconstruct the time course of a simulated source was found to be of similar accuracy for MNE versus MEM as demonstrated using SE metric. This was an important result for MEM since it was the first time the ability of MEM to recover accurate time courses of the underlying sources was assessed. Such a characteristic in MEM behavior was far from obvious since MEM is a non

linear estimator and sources for every time samples are estimated independently with no constraints on the reconstructed time course.

Chapter 4
Resolution kernel analysis

4.1 Rationale

This chapter is an introduction to the implementation of a statistical map proposed in chapter 5. We want to characterize the performance of the MEM operator per se in term of spatial accuracy, before proposing a test statistic dedicated to assess the spatial extent of the generators. If the spatial accuracy of the MEM operator is too low, this would systematically over-estimate the spatial extent of the underlying source, whatever the proposed test statistic.

Assessing the intrinsic spatial accuracy of a source localization method is usually done by analyzing the so-called resolution matrix [59, 44, 64]. Such an approach was proposed to compare the spatial accuracy of different source localization methods in EEG or in MEG.

Liu and colleagues used the resolution matrix analysis to evaluate the spatial resolution as a function of the number of EEG versus MEG sensors [59]. They also did a Monte Carlo simulation to measure the effect of the prior information based on fMRI data on a minimum norm solution. They showed that, surprisingly, EEG localization was more accurate than MEG localization for the same number of sensors averaged over many source locations and orientations. Moreover, they proved that the combination of EEG and MEG improved the spatial localization.

Finally prior fMRI constraint was shown to reduce the extent of the point spread function.

The spatial resolution of combined EEG-MEG for minimum norm estimate was also studied in Molins et al., 2000 [64]. They proposed to study two metrics estimated from the resolution matrix, i.e. the spatial dispersion and the distance localization error. They showed that the use of both EEG and MEG data improved the performance of minimum norm estimate in term of spatial dispersion and distance localization error, as compared when using MEG alone. The findings based on simulation data were validated on real data using a median nerve stimulation paradigm. The authors compared the MNE source reconstruction of the evoked response to the corresponding equivalent current dipole solution.

The resolution of the minimum norm estimate and the noise-normalized methods dSPM and sLORETA (cf. section 5.1) were compared in Hauk et al., 2011 [44]. The authors showed that the noise-normalized methods had a better localization (in term of localization error) but a larger dispersion of the point spread function than the minimum norm estimate.

The estimation of the resolution matrix is direct when dealing with linear source localization methods. However, for non-linear technique such as MEM, there is no analytical formulation of the resolution matrix and it has to be estimated numerically, which is the main objective of this chapter.

4.2 Materials and methods

Our goal was to compare and evaluate distributed methods. One way to proceed was to analyze the resolution matrix.

4.2.1 Definition

As showed in section 3.2.1, the solution for methods based on the Tikhonov regularization is of the form of the equation 3.7. By neglecting the measurement error E, we have $M = GJ$. Therefore the link between the estimate $\hat{J}$ and the true amplitude distribution J is given by:

$$\hat{J} = \underbrace{(G^T G + \lambda \Sigma_J)^{-1} G^T G}_{R} J = RJ \tag{4.1}$$

where R is by definition the resolution matrix associated with the corresponding linear source localization method. R provides the information about the inherent spatial error made by a model.

Two different types of analysis can be investigated when characterizing R:

- The columns of R are the point spread functions (PSF), i.e. the solution of the source localization method for the activation a dipolar single generator, with no noise. An ideal case would be if $R = I$, where the point spread function does not spread at all. However, it is never the case: the solution is spatially blurred and sometimes also wrongly localized. The spatial accuracy of a source localization method can then be evaluated by quantifying the blurriness and accuracy of these reconstructions.
- The rows of R represent the crosstalk functions (CTF) characterizing the influence of a single generator on the estimation of the amplitude of the other generators in its neighborhood.

One can show, using the Woodbury matrix identity [93] that

$$\hat{J} = (G^T G + \lambda \Sigma_J)^{-1} G^T M = \Sigma_J G^T (G \Sigma_J G^T + \lambda I)^{-1} M \tag{4.2}$$

This mathematical trick is very helpful for the computation of the minimum norm solution. Indeed, it will result in the inversion of a matrix of dimension $n_s \times n_s$ instead of $n_d \times n_d$, which reduces the time of computation and the memory needed to perform this operation. Using equation 4.2, we obtained:

$$R = (G^T G + \lambda \Sigma_J)^{-1} G^T G = \Sigma_J G^T (G \Sigma_J G^T + \lambda I)^{-1} G \tag{4.3}$$

Since Σ_J is symmetric, R is symmetric for source localization methods using Tikhonov regularization. This means that the PSF and the CTF for these methods are the same, which is not the case for nonlinear technique such as MEM.

Four metrics were proposed to characterize the resolution matrix. The first two metrics, the average PSF map (APM) and the average CTF map (ACM), were proposed by Liu and colleagues [59]. Let $R_{i\cdot}$ and $R_{\cdot j}$ be respectively the ith row and the jth column of the R matrix. To represent the PSF and CTF for each generator, we can define APM and ACM as the mean of each normalized columns (for APM) and rows (for ACM) of the resolution matrix.

$$APM_i = \frac{1}{n_d} \sum_{j=1}^{n_d} \frac{R_{ij}}{R_{jj}} \tag{4.4}$$

$$ACM_j = \frac{1}{n_d} \sum_{i=1}^{n_d} \frac{R_{ij}}{R_{ii}} \tag{4.5}$$

These metrics were proposed to assess the spatial accuracy of a source localization method. The lower the APM and ACM are, the more accurate the source localization technique at a specific location is.

Two other metrics, proposed in [44] and [64], were also considered in our present study:

- The dipole localization error (DLE), which is the euclidean distance between the maximum peak of the point spread function and the true activated generator. An ideal case would be when DLE = 0, meaning that the maximum of amplitude is located on the activated generator.
- The spatial dispersion (SD), for each dipole i is computed as:

$$SD_i = \sqrt{\frac{\sum_{j=1}^{n_d} d_{ij} R_{ij}^2}{\sum_{j=1}^{n_d} R_{ij}^2}} \tag{4.6}$$

  with d_{ij} being the distance between generators i and j. This metric was proposed to characterize the spatial spread of a source localization method.

4.2.2 Estimation of the resolution matrix for non-linear source localization techniques

As demonstrated in the previous section, the estimation of the resolution matrix R is straightforward for linear source localization operators. Its estimation does not require the use of any data and an analytical form of R is available. R

was estimated using the lead field matrix G and the regularization matrix Σ_J, that the Bayesian framework showed to be linked to the model of the covariance of the generators (see section 3.2.2). The hyperparameter λ was computed by using the L-curve technique. The On the other hand, such an analytical solution does not exist for non linear source localization, as it is the case for MEM-based approaches.

However, one could still estimate this resolution matrix using noise-free simulations of single dipolar generators. We could construct the resolution matrix column by column, by computing the source localization of a simulation including a single activated generator, for each generator in the cortical surface. Indeed, if we assume $\hat{J} = RJ$, then for $J = I_i$, where I_i is a vector with 1 in the ith element and 0 otherwise, the solution to the inverse problem becomes:

$$\hat{J}_i = RI_i = R_i \tag{4.7}$$

By calculating $\hat{J}_i$ for all the generators, we can obtain an estimation of R.

In the context of the MEM framework, one can be also interested in assessing the influence of the choice of the reference distribution $d\mu$ on the spatial accuracy of the MEM reconstruction. To do so, given the signal M_i corresponding to each source i [1] , a reference distributions $d\mu_i$ could be estimated. To test the influence of the reference distribution on the spatial accuracy, $\hat{J}_i$ was calculated using either

1. we can note that $M_i = GJ_i = G_i$

the reference distribution $d\mu_i$ or another one, $d\mu_j$, corresponding to M_j, the signal of a generator far from the actual activated generator. The mean geodesic distance between the actual source and the one considered to generate the reference was set to 100mm.

We also used this framework to evaluate the impact of the number and size of clusters used to initialize $d\mu$ on the resulting MEM spatial accuracy. To do so, we selected data generated by one single generator (M_i) and evaluated MEM reconstruction using brain parcelization with different number of clusters ranging from 38 (scale of 5) to 147 (scale of 3). The scale is the distance in term of degree of neighborhood (where connected nodes have a degree of neighborhood of 1) between the seed of the cluster and the generators delimiting its borders.

We used these estimated R matrices in the different configurations mentioned above to compare the spatial accuracy of MEM, cMEM and MNE.

4.3 Results

The distribution of APM, ACM, DLE and SD metrics over all possible dipole positions along the cortex are presented using boxplot representations, for each source localization method (MNE, MEM and cMEM) in Figure 4–1. It is worth noting that to facilitate the visualization, the outliers obtained in the distributions of APM and ACM metrics were removed. A value was considered as outlier when it is greater than $q_3 + 1.5(q_3 - q_1)$, where q_1 and q_3 are the 25th and 75th percentiles. For all the three methods, most of the outliers lay around 1. However some outliers for MEM and cMEM were of much larger amplitude (up to 700), revealing that these methods sometimes mislocated the single source generators.

Indeed we noticed that these outlier values corresponded only to deep generators. As expected, the values of APM and ACM for MNE were identical. On the other hand, for both MEM and cMEM the average crosstalk map median was lower than the average pointspread map. Overall we found lower ACM and APM values for MEM and cMEM when compared to MNE, suggesting that the spatial resolution was higher for MEM and cMEM. Dipole localization error was lower for cMEM as compared to MEM, itself lower than MNE. MEM and cMEM showed also overall less spatial dispersion of the PSF when compared to MNE results.

The results using the spatial clustering obtained from another generator located at 100 mm from the source of interest are illustrated in Figure 4–1. Visually one can see that the values of the metric using this clustering is very similar to the ones using the clustering from the dipole of interest, just confirming the fact that the accuracy of the parcelization had low impact on the accuracy of the results. It is worth noting that both those clusterings have a similar number of parcels (the spatial scale of the parcelization was set to 3).

A detailed example is illustrated in Figure 4–2. The idea was to estimate the best result that the source localization techniques could produce given a spatially extended source. To do so, we simulated an epileptic source in the right posterior temporal region. This source was composed of 42 dipolar generators. We summed the PSF maps corresponding to all dipoles of the simulated source; for linear techniques, it is considered as the best solution, because the spatial resolution cannot be lower. The resulting maps obtained for each source localization method were thresholded using Otsu's method [73]. For MEM and cMEM, we also evaluated

the impact of the spatial scale of the parcelization of the cortical surface on the localization results. Therefore the study was performed with scale 3 (Figure 4–2(c)), scale 4 (Figure 4–2(d)), scale 5 (Figure 4–2(e)), and scale 6 (Figure 4–2(f)). The higher the space scale, the larger the parcels were. A visual examination showed that the size of the clusters had very little influence on the accuracy of the results. Results obtained with MNE were clearly more spatially spread than results obtained with MEM and cMEM.

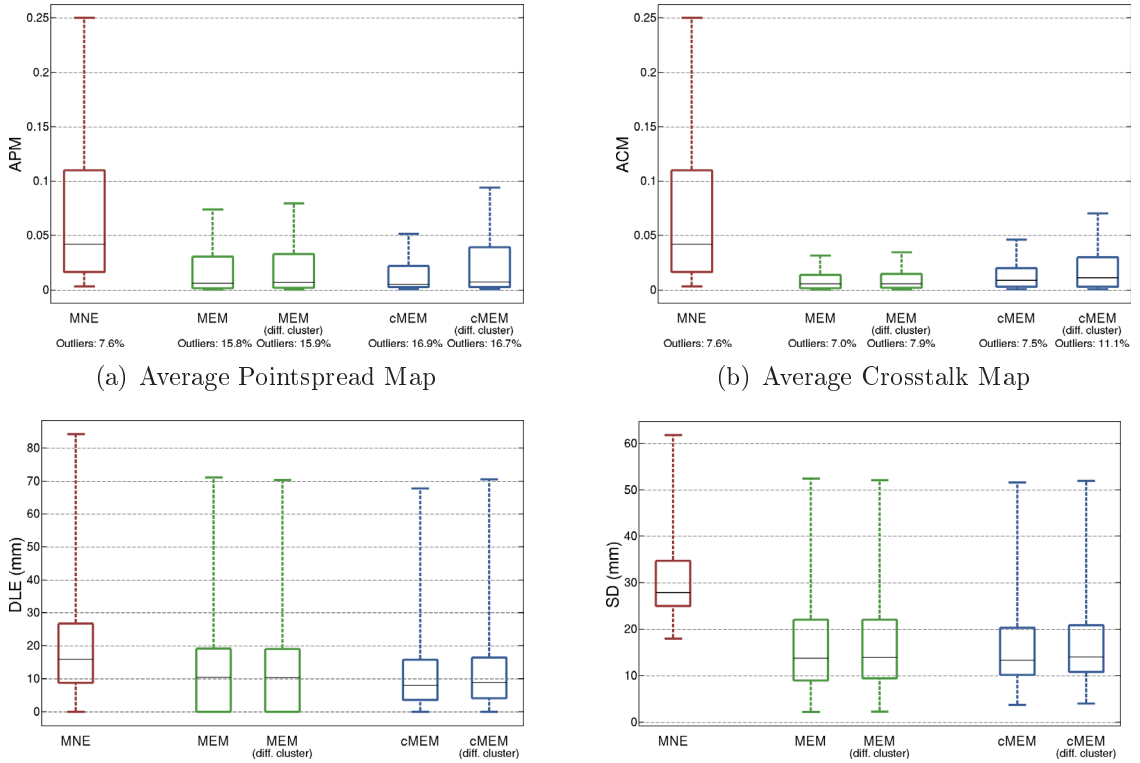

(a) Average Pointspread Map

(b) Average Crosstalk Map

(c) Dipole Localization Error

(d) Spatial Dispersion

Figure 4–1 – Boxplots of Average Pointspread Map (APM), Average Crosstalk Map (ACM), Dipole Localization Error (DLE) and Spatial Dispersion (SD) for MNE, MEM and cMEM over all the generators on the cortical surface ($N = 4203$). For MEM and cMEM, the results of the metrics when using a clustering from a generator far from the source are represented as "diff. cluster". For APM (a) and ACM (b), the outliers (whose values are larger than $q_3 + 1.5(q_3 - q_1)$, where q_1 and q_3 are the 25th and 75th percentiles) are not shown in the graph. The percentage of outliers is presented below each column.

4.4 Discussion

In this study we proposed the first analysis of the MEM solver using the resolution matrix. Even if an analytical solution cannot be found for this nonlinear technique, it is still possible to estimate the resolution matrix, by estimating explicitly the Point Spread Functions corresponding to all the dipolar generators distributed along the cortical surface. The metrics of the average point spread function and crosstalk maps gave indication of the spatial resolution of the method and offered the possibility to compare MEM with more standard solvers, such as the minimum norm estimate. We could see in Figure 4–1 that MEM solver showed both improvements for the point spread function and the crosstalk maps. The point spread function was less extended, meaning that the spatial accuracy was higher. We demonstrated that the MEM solver was able to localize focal sources with good spatial resolution, while generating very few spurious sources. The fact that MEM localizations usually provided little spurious activity is probably linked to the fact that entropy-based regularization is able to shut down the cortical parcels not contributing to the data. This is an advantage over dSPM and sLORETA which, by construction, only reduce PSFs and have the same crosstalk functions as MNE [44]. However, for MEM and cMEM, APM and ACM show few more outliers than MNE, with results up to a value of 700 (even if the numbers of outliers for MEM and cMEM are up to 17%, less than 1% of the whole number of generators are a APM and ACM greater than 1). These aberrant results affected only very deep generators, where MEG source localization were very unlikely to be

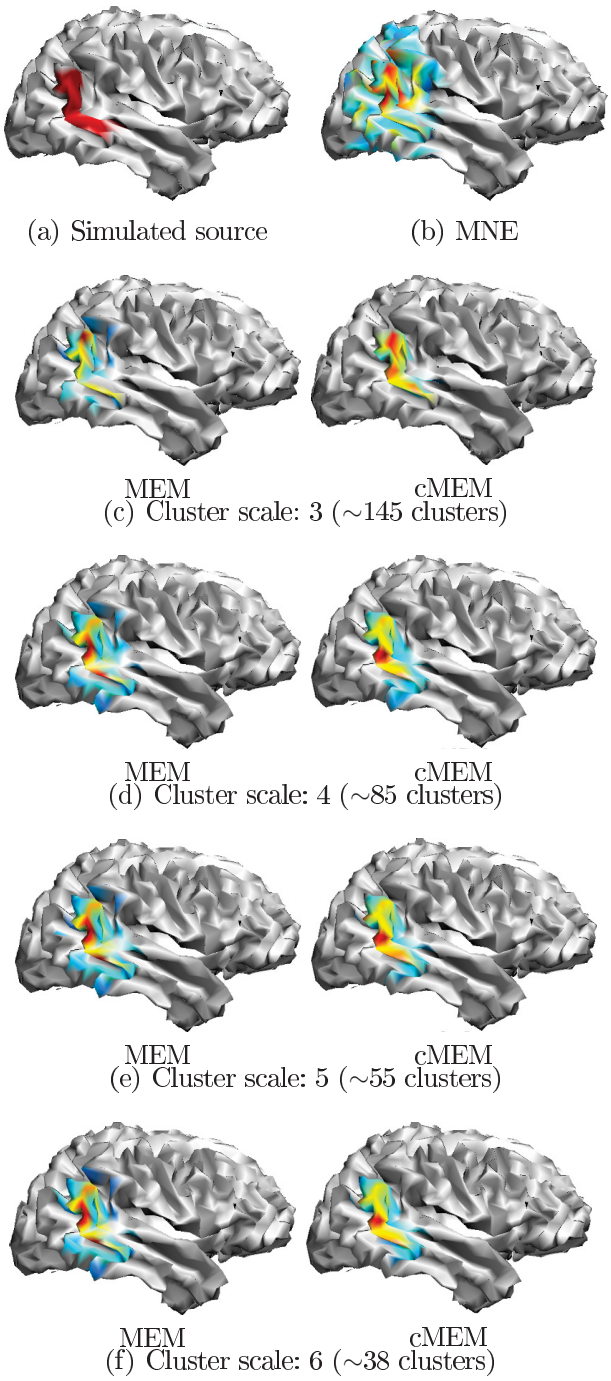

Figure 4–2 – Simulation of an extended source and "ideal" results for MNE, MEM and cMEM. These "ideal" results were obtained by adding the point spread functions of all the generators composing the source. All the maps of activity were thresholded using Otsu's method. For MEM and cMEM, the results were computed using a reference distribution $d\mu$ defined with a brain parcelization obtained at different spatial scales: scale 3 (about 145 clusters, mean area: 9.51 mm^2), scale 4 (about 85 clusters, mean area: 16.45 mm^2), scale 5 (about 55 clusters, mean area: 25.43 mm^2) and scale 6 (about 38 clusters, mean area: 36.80 mm^2).

used, and were not found for the DLE and SD scores, revealing that it was only a problem due to the normalization of APM and ACM maps.

We showed that the localization (with DLE, Figure 4–1(c)) and spatial dispersion (with SD, Figure 4–1(d)) of the point spread function were improved for MEM and cMEM when compared to MNE.

This means that for focal sources, the source localization results of the entropic techniques is of better accuracy in term of localization and spatial extent than MNE. For that reason, the MEM framework seems to be a good candidate for a source localization on which a method estimating the spatial extent of the source can be applied. Noise-normalization techniques such as dSPM and sLORETA have a lower localization error than MNE (especially for sLORETA, where DLE of the PSFs is by construction set to 0 [76]); the SD was generally lower for the unnormalized MNE, meaning that the spatial accuracy decreases for dSPM and sLORETA as the PSFs are more spatially spread.

According to our findings, both the number of clusters (Figure 4–2(c)-(f)) and the data used to estimate the clustering of the reference distribution $d\mu$ had negligible influence on the results of MEM and cMEM. This means that MEM regularization techniques are not sensitive to the accuracy of the underlying clustering needed to define the brain parcelization. This finding is consistent with what was shown in Chowdhury et al., 2013 [16]. She demonstrated that, for MEM and cMEM, the AUC score of the source localization of a simulated interictal source does not depend on the size of the spatial clustering used in the reference distribution. Therefore, the present findings are reassuring since they

are in agreement with our previous study, suggesting that the accuracy of the parcelization is not critical in the regularization of these MEM-based models.

Chapter 5
Implementation of a bootstrap-based statistical threshold in the time-scale domain

5.1 Rationale

The main goal of this section is to represent the activity of the brain not by the current density map, but by a dimensionless statistical quantity. Indeed, statistical maps have the advantage of providing a natural way of thresholding the reconstructed estimates.

Methods converting source localization methods exist. The two most popular are dSPM [20] and sLORETA [76].

5.1.1 Dynamic statistical parametric neurotechnique mapping (dSPM)

Given the equation 3.1, if we assume that J is not a random variable and $E \sim \mathcal{N}(0, \Sigma_E)$, i.e. the noise follows a zero-mean Gaussian distribution of variance Σ_E, then:

$$M \sim \mathcal{N}(GJ, \Sigma_E) \tag{5.1}$$

By combining this equation and 3.7, we have

$$\hat{J} \sim \mathcal{N}(HGJ, H\Sigma_E H^T) \tag{5.2}$$

with $H = (G^T \Sigma_E G + \lambda \Sigma_J)^{-1} G^T \Sigma_E$.

Under the null-hypothesis, assuming that the MEG signal is not affected by any activity of interest (i.e. $J = 0$), we obtain:

$$\hat{J}_{H_0} \sim \mathcal{N}(0, H \Sigma_E H^T) \tag{5.3}$$

Let C be $H \Sigma_E H^T$. A t-value map can be obtained for each generator i at a time τ using the following formula:

$$t_{\text{dSPM}}(i, \tau) = \frac{\hat{J}_{i\tau}}{\sqrt{C_{ii}}} \tag{5.4}$$

where C_{ii} is the ith element of the diagonal of C. Once all the t-values are calculated, we can obtain a statistical map. Active generators are then found by thresholding the map. The threshold can be related to a p-value using a table of values from Student's t-distribution.

5.1.2 Standardized low resolution brain electromagnetic tomography (sLORETA)

In sLORETA method, we add variability of the generative matrix with the assumption that $J \sim \mathcal{N}(0, \Sigma_J)$. The inverse solution becomes:

$$\hat{J} = (G^T \Sigma_E G + \lambda \Sigma_J)^{-1} G^T \Sigma_E M = HM \tag{5.5}$$

The variance of J influences the variance of the estimation as well:

$$C = H(\Sigma_E + G\Sigma_J G^T)H^T \tag{5.6}$$

The calculation of the t-values is proceeded in the same way as for dSPM. The generator covariance cannot be calculated and should be set using models and prior information. Most of the time, the sensor noise covariance is fixed to $\Sigma_E = I$.

dSPM and sLORETA are commonly used by researchers [74, 40, 53, 43] and are known to have a good behavior in term of localization of the source reconstruction. However the value of C_{ii} can be very small for deep generators and can lead to spurious activity in deep regions.

5.1.3 Non-parametric statistical analysis

A non-parametric statistical test refers to statistics that do not assume that the data follow any known distribution. The objective of this approach is to provide an empirical estimate of the underlying null-hypothesis distribution $H0$. This estimate of $H0$ could then be used to perform statistical tests. One way to empirically estimate the $H0$ distribution with minimum assumptions for validity is to use resampling techniques. Resampling techniques consist in using the data itself to validate a model or perform a statistical test. Resampled data are created by selecting randomly samples from the original data (the samples could be time samples, time segments, Fourier or wavelet coefficients, etc.). If those samples are drawn with replacement, it is called bootstrap [25]; if this is a sampling without replacement, the method is called permutation[46]. The estimation of $H0$ is done by computing a large number of resampled data. One of

the main disadvantages of these techniques is that they are computer intensive. On the other hand, they rely on less assumptions than classical parametric methods. Nonparametric permutation tests are often used for statistical analysis of data from functional neuroimaging experiments in PET, SPECT and fMRI [68]. In MEG, bootstrap resampling approaches have been proposed for group study analysis [12] or condition-based experiments [80, 95].

Pantazis and colleagues developed a non-parametric statistical analysis of MEG sources based on permutations between pre- and post-stimulus time segments [75]. He compared this method with the Random-Field method [94], which is based on a topological approach, in order to control the familywise error rate, i.e. the probability of making one or more false discoveries, due to the multiple comparison problem. They demonstrated that their method provided better result in term of sensitivity than Random-Field method, and does not rely on the assumptions of relative smoothness and Gaussian distribution (assumptions which are not respected by real data). Moreover, when using Random Field theory, a spatial smoothness operator is often applied to the data, thus reducing the spatial resolution.

In this chapter we propose to develop and validate a non parametric statistical test dedicated to threshold MEM based source reconstructions. The idea is to estimate the distribution of the amplitude of the source signal for each generator during baseline, i.e. without any signal of interest. We used non-parametric statistical test in order not to make any assumption of the distribution of source signal.

5.2 Materials and methods

5.2.1 Resampling method

After using MEM source localization to the MEG data, Bootstrap resampling was applied to baseline data to have an estimation of the null-hypothesis distribution for each generator. Bootstrap was used rather than permutation because it relies on fewer assumptions than permutation [25]. The sampling technique was applied on time-frequency boxes obtained with discrete wavelet representation. The analysis was performed in the time-frequency domain for three reasons:

- MEG normal brain activity has a $^1/_f$ spectral structure [31], that is intrinsic to synaptic communication [11]. Therefore in order to preserve the spectral pattern for the resampled data, it was preferable to work in the time-frequency domain.
- Bootstrap resampling is based on the resampling of independent samples. Even though it is possible to apply this technique in the temporal domain [25], in the present case the MEG time samples would not respect the assumption of independence considering the high energy in the low frequency bands for MEG background data. On the other hand, since we used discrete wavelets, the boxes in the time-frequency domain are by construction independent from each other [49], which make them reliable candidates for bootstrap resampling.

This section presents only preliminary results. Therefore, the presented method was only applied to cMEM.

The resampling technique is summarized in Figure 5–1 and was done as follows:

1. cMEM was first applied to a time window selected around the activity of interest, i.e. here, the interictal spike to localize.
2. Source localization was also apply to 2-second data of MEG background activity, or baseline. It is assumed that during the duration of the signal, no epileptic signal of interest would occur. However the initialization of the cMEM for this baseline localization was a bit different. Instead of calculating the reference distribution $d\mu$ based on the data, we used the reference distribution estimated when localizing the peak of the signal of interest in order to initialize α_{init}. The clusters, the values of α_{init}, μ_k and Σ_k are therefore the same for both localizations (the spike of interest and the baseline). We used the same $d\mu$ for the localization of the baseline and the signal of interest because, in order to provide a statistical threshold, we were interested in the difference between the source reconstruction of the signal of interest and the reconstruction of the background activity, given the same prior distribution.
3. A discrete wavelet-transform was applied to the result of the baseline localization. We used here Daubechies wavelets [49] because they are able to remove polynomial trends in the signal. In our context, we used wavelets with four vanishing moments, meaning that the wavelets are able to get rid of 3-polynomials present in the signal. The frequency domain is represented by scales, which is equivalent to frequency bands. A time-scale representation

was obtained for each generator of the cortical surface and along the 2-second baseline.

4. This time-scale representation was resampled N_s times. The resampling follows the following rules:
   - For each resampling realization, the same bootstrap resampling strategy was applied for all the generators to preserve the same spatial and spectral structure in the overall signal.
   - The time-scale boxes corresponding to the first and last 5% of the time samples were left untouched to avoid side effects.

   Therefore, in the original data, for each frequency scale, the coefficients of the resampled data were randomly drawn (with replacement) from the set of the original coefficients. The resampling strategy (e.g. "the first resampled coefficient is the third original coefficient, the second resampled coefficient is the first original coefficient, etc.") was reproduced for all the generators.
5. For each resampling realization, an inverse wavelet-transformed was applied.
6. For each source, the amplitude values of all the resampling realizations for each time sample were taken and put into a histogram.
7. The current value of the reconstruction during the peak of the signal of interest was compared to the histogram and a p-value $\hat{p}$ was estimated, corresponding to the ratio between the number of elements in the histogram larger than that number and the total number of elements ($T \times N_s$). If

H_i represents the values of the estimation of the distribution of the null-hypothesis for generator i, then:

$$\hat{p}_i = \frac{\text{card}(H_i > J_{cMEM}(i, t_{\text{peak}}))}{\text{card}(H_i)} \tag{5.7}$$

8. The multiple comparison on the source space was handled by a False Discovery Rate (FDR) technique [7]. To do so, the p-values P were ordered from the smallest to the largest value $(\hat{p}_{(1)} \leq \hat{p}_{(1)} \leq \cdots \leq \hat{p}_{(n)})$, considered as active all the sources which followed:

$$P_{(i)} \leq \frac{i}{n_d}\alpha, \tag{5.8}$$

with $\alpha = 0.05$ the expected FDR rate.

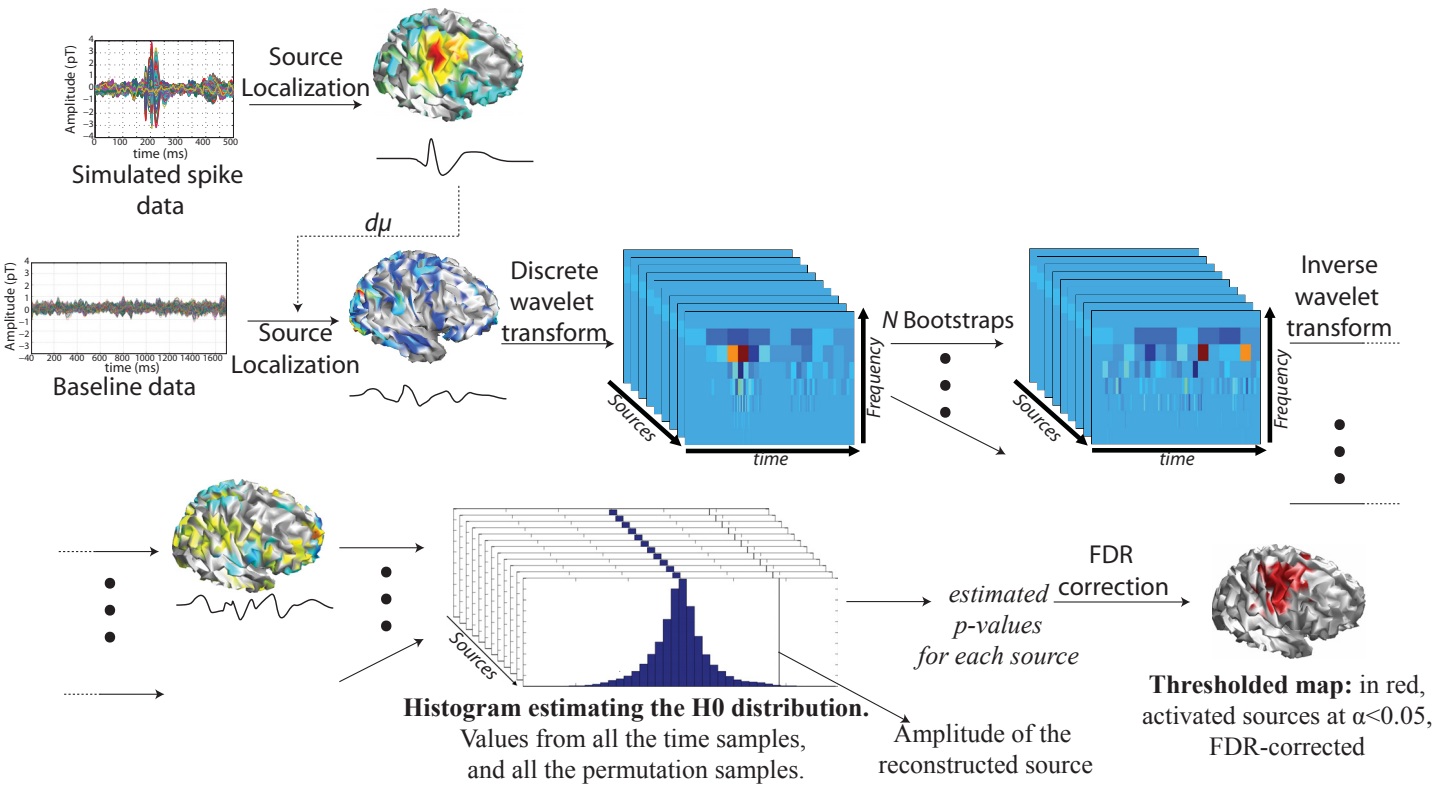

Figure 5–1 – Illustration of the procedures used to produce statistical map. First, the source localization was performed on the simulated signal using cMEM technique. Then we apply the cMEM technique on a background signal of MEG activity using the same reference distribution as for the simulated source localization. A discrete wavelet transform is applied on the resulting density map. For each generator, we obtain a time-scale map composed of a finite number of time-frequency boxes. A bootstrap technique is performed on the time-frequency boxes, independently for each scale. This operation is repeated N times (here, N = 1000). The inverse discrete wavelet transform is used to obtain N time-varying current density map. For each generator, the amplitudes for all the time samples and all the bootstrap samples are used to construct an estimate of the null-hypothesis density function for this generator. The amplitude of the reconstructed source is compared to the histograms and p-values are obtained. After FDR correction and given a significance rate $\alpha = 0.05$, a statistical map is obtained.

5.2.2 Simulation and evaluation

Interictal spikes were simulated on 5 different localizations on the cortical surface (see Figures 5–4 and 5–5). Simulations were made with two spatial extents (one small, $\sim$7cm^2, and one large, $\sim$25cm^2). 5 different segments of 2 seconds of baseline, taken from data showing no clear epileptic discharges, were added to the simulated data as realistic noise, with a constant SNR of 2, for a total of 50 datasets. The source localization was performed on single trials. The resampling method was applied and we obtained, for each localization with a particular noise segment, an estimated $H0$ distribution for each generator, and a statistical map of activated generators.

5.3 Results

Figure 5–2 shows the result of cMEM for a simulation on the left fronto-opercular region. The figure also shows the estimations of the $H0$ for two generators located within the simulated source, the seed of the source and one located on the edge of the simulated source, and two other generators, one close to the actual activated source, the other located on the contra-lateral hemisphere. We can see all the distributions resemble Gaussian distributions, but we observed a large variability of the standard deviation of these distributions. The largest standard deviation was observed for the seed of the source. The other generator within the simulated source, even if it was close to the seed point, had a very low standard deviation, because it was deeper in the cortex, as you can see in Figure 5–3. The same reason is probably the cause of the low standard deviation of the remote generator.

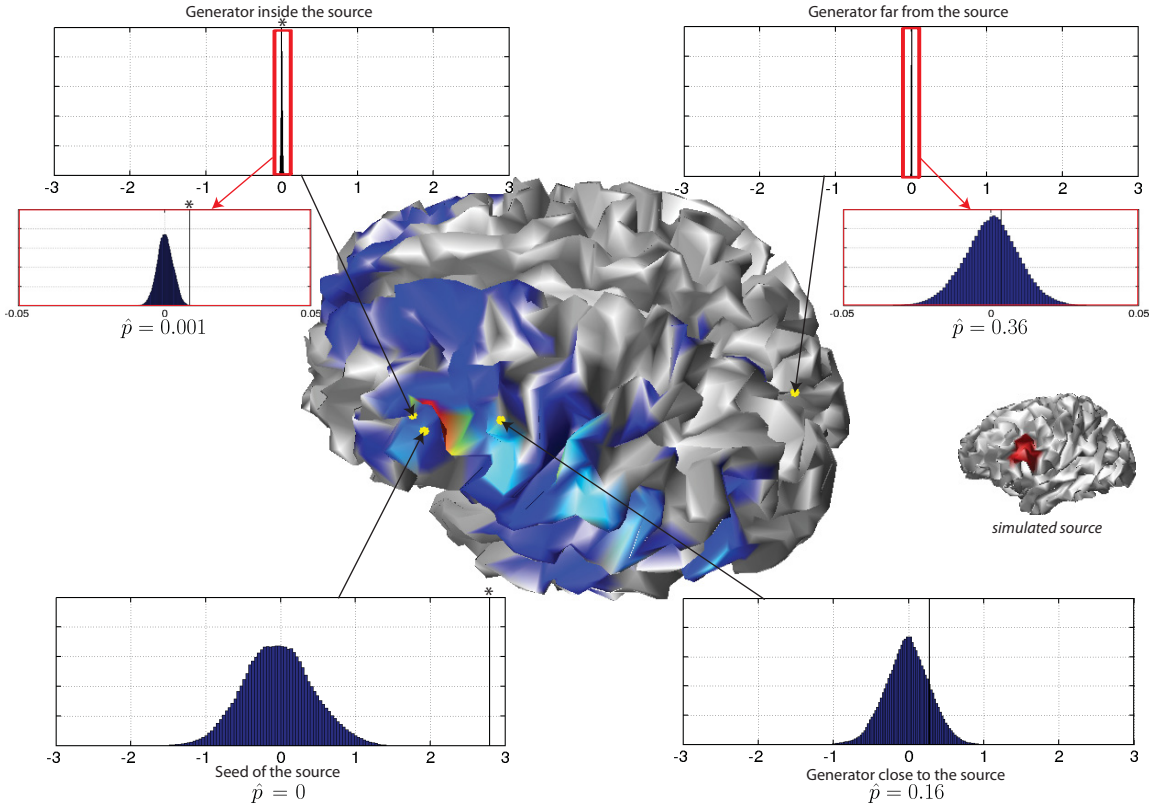

Figure 5–2 – cMEM reconstruction of a simulated source, and estimated $H0$ distribution for some of the generators. The black line represents the amplitude of the reconstruction, the asterisks indicate when the generator is significantly different from the null hypothesis ($\alpha < 0.05$, FDR corrected). The red graphs are magnified representations of the distributions.

The map of all the standard deviation of the estimated $H0$ distribution for all the vertices along the cortical surface was illustrated in Figure 5–3. We can see that the maximum of variance was located near the simulated source, and on superficial generators.

The summary of the results for all the simulations is illustrated in Figures 5–4 (small spatial extent, $\sim$7cm^2) and Figure 5–5 (large spatial extent, $\sim$25cm^2). The

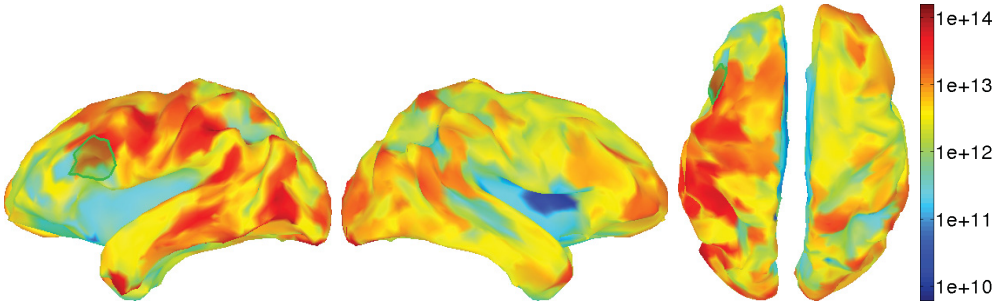

Figure 5–3 – Spatial map of the estimated standard deviation of the $H0$ distribution in $(\text{pA.m})^2$. The data are shown in a logarithmic scale. The maximum of variance is located near the simulated source, on superficial generators.

statistical maps were compared to the actual activated generators. The metrics of sensitivity (proportion of true positive, i.e. simulated generators found as activated on the statistical map) and specificity (proportion of true negative, i.e. non-simulated generators found as non-activated on the statistical map) are presented. For specificity, we proposed to separate the generators close to the source from the others. A generator is considered as close if it is located at 10 or fewer degrees of neighborhood from an activated generator, i.e. up to about 65mm from the source in term of geodesic distance along the cortical surface.

For some maps in Figure 5–4 nothing was found significant, leading to sensitivity of 0 and specificity of 1. We can see in Figure 5–4 that the sensitivity is often high (above 0.7) whereas the specificity, especially the one for close generators, was quite low, meaning that the spatial extent of the source seems to be overestimated. For sources of larger extent, the specificity of close generators rarely reaches 0.5. The segment of baseline used as noise greatly affects the results,

and the values of sensitivity and specificity are varying a lot from one noise segment to the other.

Examples of the statistical maps are illustrated in Figures 5–6 and 5–7. It shows the simulated source, its localization, the resulting statistical map and the localization when using the activated threshold as a mask, for both spatial extents. The Figure 5–6 corresponds to the results of the simulation on the first row and third column of Figures 5–4 and 5–5, and Figure 5–7 corresponds to the simulation on the third row and second column. We can see that for all these results, the source of activity was found activated. However the spatial extent was greatly overestimated, with an obvious example presented in Figure 5–7(g) where almost all the hemisphere was found activated, which shows that some statistical maps behave better than others.

Figure 5–8 shows the results of α_{init}, i.e. the initial value of the mean of the activated generators for MEM source localization, used for the source and the baseline localizations. The map should be compared to the results of the statistical map of the Figures 5–6 and 5–7. For both maps 5–8(b) and 5–8(d), the larger values of α_{init} cover much more that the simulated source, which is an expected result. α_{init} comes from MSP values [61], which is an unspecific prelocalization which does not mean to be focal. One can notice that many more dipoles are showing large values of α_{init} in example 2 (Figure 5–7) than in example 1 (Figure 5–6). On the other hand, the values of specificity were higher for the statistical map corresponding to example 1 (see Figure 5–6) rather than example 2 (see Figure 5–7), even if a large spurious activity can be found in the left insula in

example 1. Those are simply preliminary results, but it seems that the amplitude and the good detection of α_{init} are related to the quality of the statistical map. Further investigation will be performed, but evaluating the influence of the α on statistical maps was beyond the scope of my Master's thesis.

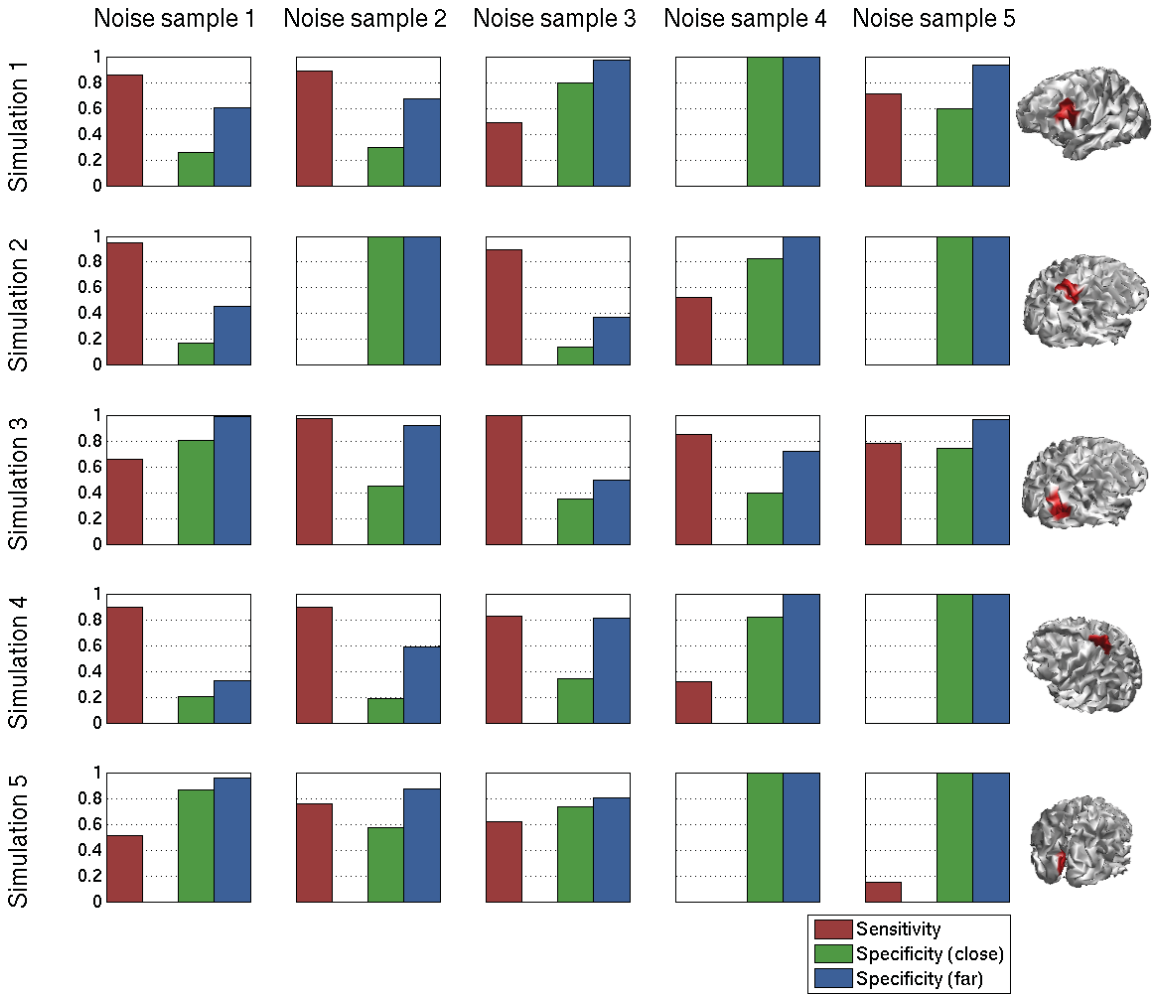

Figure 5–4 – Evaluation of the statistical map for 5 small sources (mean size: 14 cm^2), for 5 different noise samples used as realistic noise. The simulated source is illustrated in the right of each row. The baseline used to estimate $H0$ was the same for all tests. The sensitivity, the specificity close to the source (a dipolar generator located within the 10th spatial neighborhood order of the seed of the simulated source), and the specificity far from the source is shown for all the configurations. It is worth noting that for 4 of these maps, the sensitivity is equal to 0, and the specificity is equal to 1, meaning that the statistical map did not detect anything significant activity.

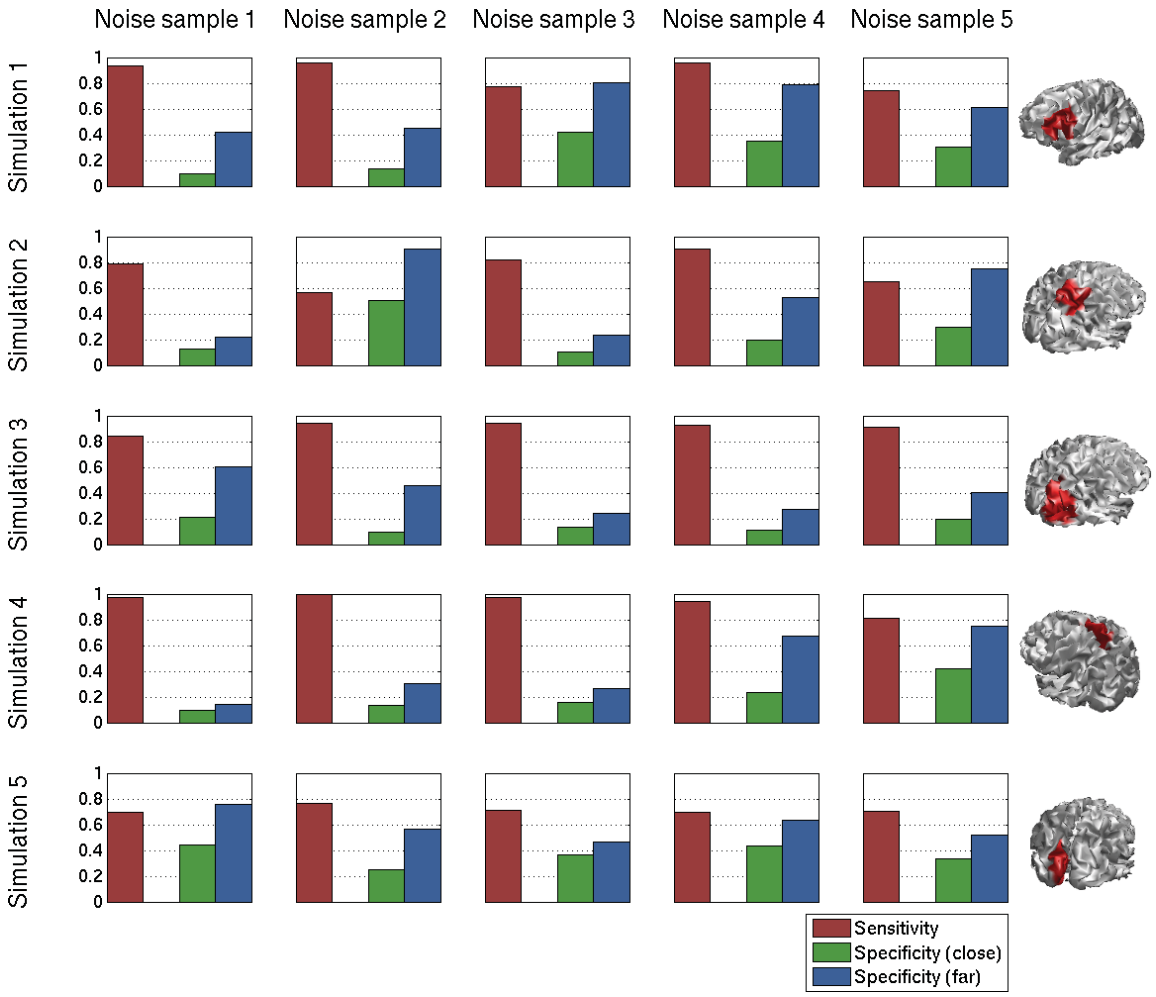

Figure 5–5 – Evaluation of the statistical map for 5 large sources (mean size: 37cm ^{2}), for 5 different noise samples used as realistic noise. The simulated source is illustrated in the right of each row. The baseline used to estimate $H0$ was the same for all tests. The sensitivity, the specificity close to the source (a dipolar generator located within the 10th spatial neighborhood order of the seed of the simulated source), and the specificity far from the source is shown for all the configurations.

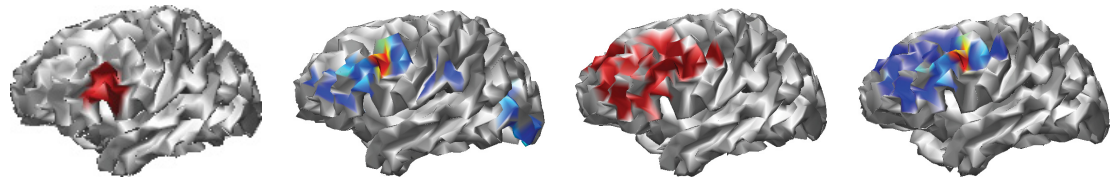

(a) Simulated source (spatial extent 3) (b) Source localization (c) Statistical threshold (d) Source localization using statistical mask

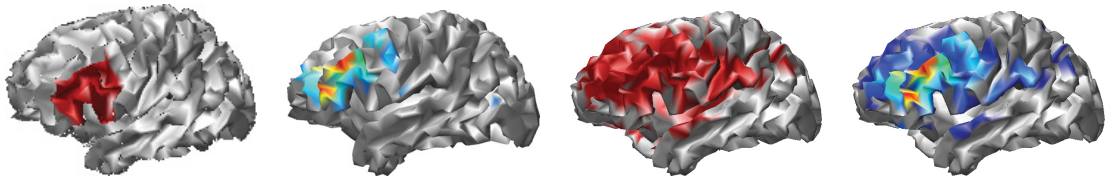

(e) Simulated source (spatial extent 5) (f) Source localization (g) Statistical threshold (h) Source localization using statistical mask

Figure 5–6 – Illustration of the statistical map for simulation 1 with noise sample 3 in Figures 5–4 and 5–5. **Top**: small spatial extent. **Bottom**: large spatial extent. (a)(e): simulated source. (b)(f): Source localization, visualization with Otsu's threshold. (c)(g): Statistical map. (d)(h): Source localization showing all the generators considered as active.

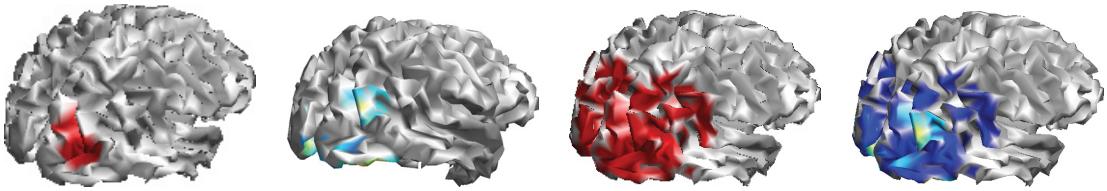

(a) Simulated source (spatial extent 3) (b) Source localization (c) Statistical threshold (d) Source localization using statistical mask

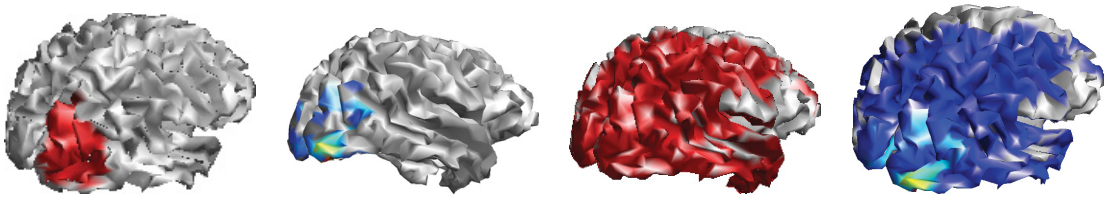

(e) Simulated source (spatial extent 5) (f) Source localization (g) Statistical threshold (h) Source localization using statistical mask

Figure 5–7 – Illustration of the statistical map for simulation 3 with noise sample 2 in Figures 5–4 and 5–5. **Top**: small spatial extent. **Bottom**: large spatial extent. (a)(e): simulated source. (b)(f): Source localization, visualization with Otsu's threshold. (c)(g): Statistical map. (d)(h): Source localization showing all the generators considered as active.

5.4 Discussion

We showed in chapter 4 that the MEM-based source localization had a greater spatial resolution than traditional methods. The goal of this chapter was to come up with a method able to perform statistical analysis on a source localization solution to obtain a map of activated generators. To do so, the current amplitude at the peak of the reconstructed solution was compared to an estimation of the $H0$ distribution for each generator. This null-hypothesis estimate was computed using the bootstrap method on the time-scale domain on baseline data. The reason why we used bootstrap on wavelet transformed data is to keep the $^1/_f$ structure of the MEG background activity.

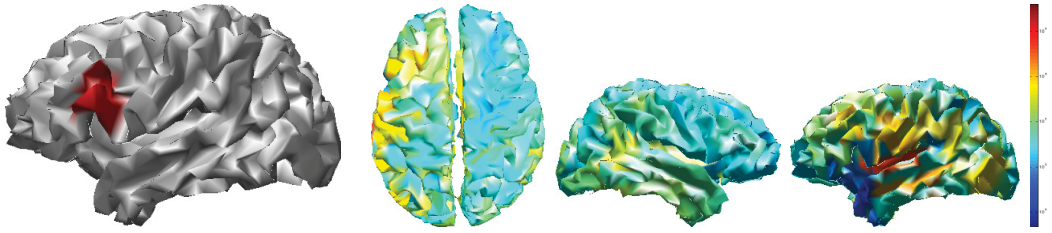

(a) Simulated source (b) Corresponding α_{init}

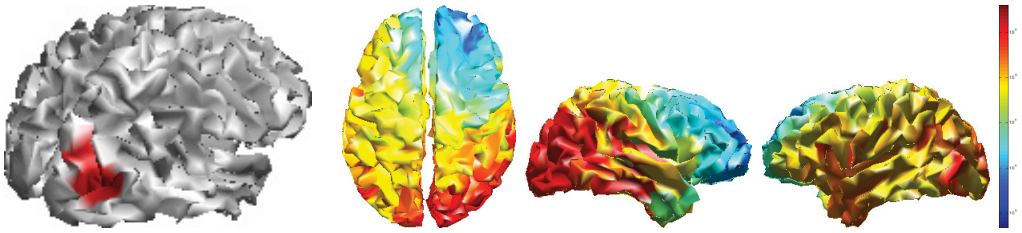

(c) Simulated source (d) Corresponding α_{init}

Figure 5–8 – Map of the values of α_{init} for two statistical analyses.

Figure 5–3 showed that the standard deviation of the $H0$ distribution was of great variability for the generators on the cortical surface. The variance of $H0$ estimate for deep dipoles is of smaller amplitude than superficial ones. Therefore it is important that, like the method proposed here, the estimated statistical threshold should be different for each dipolar generator. From results not shown in this study, we saw that the segment of baseline used to make the bootstrap samples was of little influence on the estimate of $H0$ standard deviations.

Based on Figures 5–4 and 5–5, we showed that our statistical analysis were sensitive and not specific: our technique was able to recover the spatial extent of the source but tended to overestimate its spatial extent, even if MEM localization seemed to correctly reconstruct the source. On the other hand, the MEM method provided an accurate source localization. The $H0$ distribution estimated for each

generator showed a great variability of the standard deviation, thus making it difficult to provide an optimal statistical map. First results suggested that the statistical thresholding was more efficient when the α_{init} was accurately estimated.

One can try to understand the reason why we were not able to find a better solution. It seems that the technique is highly affected by the determination of the reference distribution $d\mu$ for MEM technique. First of all, the statistical map is affected by the background activity of simulation for the source localization (columns in Figures 5–4 and 5–5). The noise sample affects, among others, the initialization of α_{init} which was used for the localization of the baseline (step 2 of the proposed technique, see Figure 5–8). This might explain why the statistical map results change so drastically with the noise sample, since preliminary investigation seems to show that the quality of statistical map is related to the value of α_{init}, a fortiori to the reference distribution $d\mu$. We need to provide methods to extract in a more robust manner the properties of H0 distribution, to show less variability with the choice of the baseline segment.

Different ways of improving the statistical analysis exist. One can think of applying the bootstrap analysis at the sensor level, as what was done in the study from Xu and colleagues [95], and to apply the baseline localization on the bootstrap samples. The result may be less affected by the reference distribution. On the other hand, the computational cost becomes extremely important since $N = 1000$ MEM localizations are now needed. This is the reason why this option was discarded and that the bootstrap samples were used on the level of the dipolar generators.

Chapter 6
General conclusion

In the domain of epilepsy, the localization of the zone of the brain triggering the seizures is primordial. The magnetoencephalography (MEG), which measures the magnetic field resulting from the brain activity, is one of the modalities used to localize the epileptogenic focus. It is based on the detection of the onset of activity of interictal spikes, transient activity occurring between the seizures. MEG has the advantage of having a higher temporal resolution than the other imaging techniques (such as fMRI and PET). However, the spatial resolution of MEG is limited, as signals are recorded from the scalp. On the other hand, MEG is less affected than EEG by the resistivity of the skull, the spatial resolution is then higher than for EEG. Distributed source localization is based on the assumption that the brain activity is generated on the cortical surface and can be approximated by a set of evenly distributed generators. Given this assumption the resolution of the source localization becomes linear, but under-determined, meaning the problem has an infinite number of solutions. To obtain a unique solution, one needs to add some additional constraints. The Maximum of Entropy on the Mean (MEM) technique is a framework which aims at finding the solution which maximizes the μ-entropy (i.e. minimizes the Kullback-Leibler divergence) to a reference distribution. Our reference distribution in this thesis is based on a data-driven full parcelization of the brain.

6.1 Spatio-temporal evaluation of reconstructed propagating sources

6.1.1 Summary

The objective of the thesis was three-fold. First, we wanted to make sure that the MEM techniques had a good ability to detect temporal propagation. Indeed, interictal spikes may propagate along the cortical surface and it is crucial to be able to recover the propagation pattern of the source to identify the onset of activity. In Chapter 3, we showed, based on realistic simulations of epileptic spikes, that the MEM techniques were able to recover the spatial extent of the source along propagation patterns. We also confirmed previous studies [36, 16] showing that MEM obtained better localization than standard techniques (such as the minimum norm (MNE) estimate). Finally we demonstrated the ability for MEM and cMEM to recover accurately the time course of the underlying sources.

6.1.2 Future work

Future works will focus on the generation of more realistic propagation patterns, using models of coupled neuronal populations [19]. Moreover, the present findings will be validated using real data, where the propagation patterns could be validated with intracranial EEG recordings.

6.2 Resolution kernel analysis

6.2.1 Summary

The second part of this study (Chapter 4) was to compare the theoretical spatial resolution of the source localization methods and especially of the MEM solver. To do so, we used different metrics based on the resolution matrix. For linear techniques, such as MNE, the resolution matrix has an analytical formula.

For MEM techniques, this matrix can be estimated based using Monte Carlo simulations of single generator source localization. By comparing the point spread functions of MEM and MNE in Chapter 4, we concluded that MEM localization was more focal and more accurate. These results mean that the spatial resolution of MEM techniques is higher. These results are really important considering the fact that we are looking for a method sensitive to the spatial extent of the source. It is the first time such an analysis is performed for MEM approaches. Besides, we showed that the size and accuracy of the data-driven parcelization used for the reference distribution in MEM and cMEM did not have any influence on their spatial resolution, thus reproducing and confirming in other conditions some of our previous findings [16].

6.2.2 Future work

Next step would be to validate the present findings using somatosensory response data, as the study proposed by Molins and colleagues [64]. This kind of study has the advantage of being easy to acquire and is known to produce focal response, which can be modeled by a single generator source. The seed of activity would be localized using a single dipole fit localization at the peak of the evoked signal obtained after electrical median nerve stimulation. The analysis of the localization and spatial extent of the source localization techniques can give us insights on the spatial resolution of those techniques.

One way of using the resolution matrix analysis is to quantify the improvement in term of spatial accuracy of fusion data. As mentioned before, Molins et al. [64] and Liu et al. [59] compared the spatial resolution of MNE using a fusion of

EEG and MEG (by concatenating the signal and gain matrices) to EEG and MEG alone. Both teams concluded that fusion had a significant impact on the accuracy of the reconstruction. Future works will investigate the effect of EEG-MEG fusion on MEM or cMEM.

6.3 Implementation of a bootstrap-based statistical threshold in the time-scale domain

6.3.1 Summary

The third part (Chapter 5) dealt with the implementation of statistical analysis to obtain a map of activated generators. To do so, for each generator on the cortical surface the null-hypothesis distribution was estimated using a bootstrap resampling technique. The bootstrap technique was used to avoid imposing any a priori on the null hypothesis distribution in the cMEM source space. The analysis was performed using discrete wavelet to keep the $^1/_f$ spectral structure of the data, and to obtain independent samples since discrete wavelet representations provide interesting decorrelation properties between time samples and scales [49]. After localization a segment of background activity, we obtained a set of time-frequency boxes, using discrete Daubechies wavelet transformed. Those time-frequency boxes were resampled to create new samples estimating baseline activity. The samples were regrouped into histograms which estimate the distribution of background activity. The source localization result was then compared to those histograms to obtain p-values statistics, and therefore a statistical map. Even if the results from Chapter 4 were really promising, the results obtained here were not as good as expected. The statistical map lacks specificity, meaning that the spatial extent is not recovered, and cannot be

estimated based on this technique. We have not clearly identified the reason of this result yet, but it is probably due to the calculation of the reference distribution. We demonstrated that the $H0$ distribution was found to be complex and highly influenced by the initialization of α for the MEM reference distribution.

6.3.2 Future work

A large part of the work remains to be done to obtain a satisfactory statistical map of activity. Moreover, the technique will be applied to a new source localization technique, the wavelet-based MEM (wMEM), which is the MEM technique applied to the time-frequency boxes of the discrete wavelet transform of the signal [58]. We expect wMEM approach to be more appropriate to these non parametric statistical approaches, since the sources are directly estimated in the time-frequency boxes during the localization procedure.

6.4 Final conclusion

Source localization is still a hot topic in EEG and MEG, and it is possible to improve the accuracy and the spatial resolution of the reconstruction. MEM is a promising technique since we proved it was able to recover the time course of sources and had a better spatial resolution than standard techniques. Few steps are left to do to obtain a statistical map to be able to give a good estimation of the extent of a source, a useful piece of information for the presurgical investigation of patients with epilepsy.

References

[1] AI Ahonen and MS Hämäläinen. 122-channel SQUID instrument for investigating the magnetic signals from the human brain. *Physica Scripta*, 198:198–205, 1993.

[2] Cécile Amblard, Ervig Lapalme, and Jean-Marc Lina. Biomagnetic source detection by maximum entropy and graphical models. *IEEE transactions on bio-medical engineering*, 51(3):427–42, March 2004.

[3] S. Baillet, J.C. Mosher, and R.M. Leahy. Electromagnetic brain mapping. *Signal Processing Magazine, IEEE*, 18(6):14 –30, nov 2001.

[4] Sylvain Baillet, J C Mosher, and Richard M Leahy. Electromagnetic brain mapping. *Human brain mapping*, 30(6):1753–7, June 2009.

[5] C Baumgartner, G Lindinger, a Ebner, S Aull, W Serles, a Olbrich, S Lurger, T Czech, R Burgess, and H Lüders. Propagation of interictal epileptic activity in temporal lobe epilepsy. *Neurology*, 45(1):118–22, January 1995.

[6] C Baumgartner, E Pataraia, G Lindinger, and L Deecke. Magnetoencephalography in focal epilepsy. *Epilepsia*, 41 Suppl 3:S39–47, January 2000.

[7] Y Benjamini and Y Hochberg. Controlling the false discovery rate: a practical and powerful approach to multiple testing. *Journal of the Royal Statistical Society. Series B ...*, 135(1):22–6, January 1995.

[8] Hans Berger. Über das elektrenkephalogramm des menschen. *Archiv für Psychiatrie und Nervenkrankheiten*, 87(1):527–570, 1929.

[9] A. Bernasconi, N. Bernasconi, B. C. Bernhardt, and D. Schrader. Advances in MRI for 'cryptogenic' epilepsies. *Nat Rev Neurol*, 7(2):99–108, Feb 2011.

[10] David A. Boas, Anders M. Dale, and Maria Angela Franceschini. Diffuse optical imaging of brain activation: approaches to optimizing image sensitivity, resolution, and accuracy. *NeuroImage*, 23(Supplement 1):S275 – S288, 2004. Mathematics in Brain Imaging.

[11] György Buzsáki and Andreas Draguhn. Neuronal oscillations in cortical networks. *Science (New York, N.Y.)*, 304(5679):1926–9, June 2004.

[12] Wilkin Chau, Anthony R McIntosh, Stephen E Robinson, Matthias Schulz, and Christo Pantev. Improving permutation test power for group analysis of spatially filtered MEG data. *NeuroImage*, 23(3):983–96, November 2004.

[13] N. Chauveau, X. Franceries, B. Doyon, B. Rigaud, J. P. Morucci, and P. Celsis. Effects of skull thickness, anisotropy, and inhomogeneity on forward EEG/ERP computations using a spherical three-dimensional resistor mesh model. *Human Brain Mapping*, 2004.

[14] Douglas Cheyne, Andreea C. Bostan, William Gaetz, and Elizabeth W. Pang. Event-related beamforming: A robust method for presurgical functional mapping using MEG. *Clinical Neurophysiology*, 118(8):1691 – 1704, 2007.

[15] R. Chowdhury. Localization of the generators of epileptic activity using magneto-encephalography (MEG) data. Master's thesis, McGill university, 2011.

[16] Rasheda Arman Chowdhury, Jean Marc Lina, Eliane Kobayashi, and Christophe Grova. MEG Source Localization of Spatially Extended Generators of Epileptic Activity: Comparing Entropic and Hierarchical Bayesian Approaches. *PloS one*, 8(2):e55969, January 2013.

[17] D. Cohen. Magnetoencephalography: Evidence of Magnetic Fields Produced by Alpha-Rhythm Currents. *Science*, 161(3843):784–786, August 1968.

[18] D. Cohen. Boston and the history of biomagnetism. *Neurol Clin Neurophysiol*, 2004:114, 2004.

[19] Delphine Cosandier-Rimélé, Jean-Michel Badier, Patrick Chauvel, and Fabrice Wendling. A physiologically plausible spatio-temporal model for EEG signals recorded with intracerebral electrodes in human partial epilepsy. *IEEE transactions on bio-medical engineering*, 54(3):380–8, March 2007.

[20] AM Dale, AK Liu, BR Fischl, and RL Buckner. Dynamic statistical parametric neurotechnique mapping: combining fMRI and MEG for high-resolution imaging of cortical activity. *Neuron*, 26:55–67, 2000.

[21] AM Dale and MI Sereno. Improved localizadon of cortical activity by combining eeg and meg with mri cortical surface reconstruction: A linear approach. *Journal of Cognitive Neuroscience*, 1993.

[22] Anders M. Dale and Martin I. Sereno. Improved localization of cortical activity by combining EEG and MEG with MRI cortical surface reconstruction: A linear approach. *J. Cogn. Neurosci*, 5:162–176, 1993.

[23] J. Daunizeau, J. Mattout, B. Goulard, J.-M. Lina, and H. Benali. Data-driven cortex parcelling: a regularization tool for the EEG/MEG inverse problem. In *Biomedical Imaging: Nano to Macro, 2004. IEEE International Symposium on*, pages 1343 – 1346 Vol. 2, april 2004.

[24] John S. Ebersole. EEG dipole modeling in complex partial epilepsy. *Brain Topography*, 4:113–123, 1991. 10.1007/BF01132768.

[25] Bradley Efron and R J Tibshirani. *An Introduction to the Bootstrap (Chapman & Hall/CRC Monographs on Statistics & Applied Probability)*. Chapman and Hall/CRC, 1 edition, 1994.

[26] R G Emerson, C a Turner, T a Pedley, T S Walczak, and M Forgione. Propagation patterns of temporal spikes. *Electroencephalography and clinical neurophysiology*, 94(5):338–48, May 1995.

[27] Jerome Engel, Timothy A Pedley, and Jean Aicardi. *Epilepsy: a comprehensive textbook*, volume 1. Lippincott Williams & Wilkins, 2008.

[28] B.S. Everitt and A. Skrondal. *The Cambridge Dictionary of Statistics*. Cambridge University Press, 2010.

[29] Robert Fisher, Walter can Emde Boas, Warren Blume, Christian Elger, Pierre Genton, Phillip Lee, and Jerome Engel. Epileptic seizures and epilepsy: definitions proposed by the International League Against Epilepsy (ILAE) and the International Bureau for Epilepsy (IBE). *Epilepsia*, 46(10):1698–9; author reply 1701–2, October 2005.

[30] Robert Fisher and Maslah Saul. Overview of epilepsy. pages 1–56, 2010.

[31] W J Freeman, L J Rogers, M D Holmes, and D L Silbergeld. Spatial spectral analysis of human electrocorticograms including the alpha and gamma bands. *Journal of neuroscience methods*, 95(2):111–21, February 2000.

[32] D Geffroy, D Rivière, I Denghien, N Souedet, S Laguitton, and Y Cointepas. BrainVISA : a complete software platform for neuroimaging. In *Python in Neuroscience workshop*, 2011.

[33] Jean Gotman. Epileptic networks studied with EEG-fMRI. *Epilepsia*, 49 Suppl 3:42–51, January 2008.

[34] A. Gramfort. *Mapping, timing and tracking cortical activations with MEG and EEG: Methods and application to human vision.* PhD thesis, INRIA Sophia Antipolis, 2009.

[35] A Gramfort, T Papadopoulo, E Olivi, and M Clerc. {O}pen{M}{E}{E}{G}: opensource software for quasistatic bioelectromagnetics. *Biomed Eng Online*, 9:45, 2010.

[36] C Grova, J Daunizeau, J-M Lina, C G Bénar, H Benali, and J Gotman. Evaluation of EEG localization methods using realistic simulations of interictal spikes. *NeuroImage*, 29(3):734–53, February 2006.

[37] LF Haas. Hans berger (1873–1941), richard caton (1842–1926), and electroencephalography. *Journal of Neurology, Neurosurgery & Psychiatry*, 74(1):9–9, 2003.

[38] M. S. Hamalainen and R. J. Ilmoniemi. Interpreting magnetic fields of the brain: minimum norm estimates. *Med Biol Eng Comput*, 32(1):35–42, Jan 1994.

[39] Per Christian Hansen. Analysis of discrete ill-posed problems by means of the l-curve. *SIAM review*, 34(4):561–580, 1992.

[40] K Hara, F-H Lin, S Camposano, D M Foxe, P E Grant, B F Bourgeois, S P Ahlfors, and S M Stufflebeam. Magnetoencephalographic mapping of interictal spike propagation: a technical and clinical report. *AJNR. American journal of neuroradiology*, 28(8):1486–8, September 2007.

[41] R Hari and E Kaukoranta. Neuromagnetic studies of somatosensory system: principles and examples. *Progress in neurobiology*, 24(3):233–256, 1985.

[42] Hideji Hattori, Naohiro Tsuyuguchi, Tsuyoshi Tsutada, Hiroshi Ishida, Katsuji Tanaka, Osamu Matsuoka, and Tsunekazu Yamano. Intra- and interhemispheric propagation of interictal spikes in epilepsy patients as measured by MEG. *International Congress Series*, 1300:645–648, June 2007.

[43] Stefan Haufe, Ryota Tomioka, Thorsten Dickhaus, Claudia Sannelli, Benjamin Blankertz, Guido Nolte, and Klaus-Robert Müller. Large-scale EEG/MEG source localization with spatial flexibility. *NeuroImage*, 54(2):851–9, January 2011.

[44] O. Hauk, D. G. Wakeman, and R. Henson. Comparison of noise-normalized minimum norm estimates for MEG analysis using multiple resolution metrics. *Neuroimage*, 54(3):1966–1974, Feb 2011.

[45] R. N. Henson, J. Mattout, C. Phillips, and K. J. Friston. Selecting forward models for MEG source-reconstruction using model-evidence. *Neuroimage*, 46:168–176, 2009.

[46] A. P. Holmes, R. C. Blair, J. D. Watson, and I. Ford. Nonparametric analysis of statistic images from functional mapping experiments. *J. Cereb. Blood Flow Metab.*, 16(1):7–22, Jan 1996.

[47] H. J. Huppertz, S. Hoegg, C. Sick, C. H. Lcking, J. Zentner, A. Schulze-Bonhage, and R. Kristeva-Feige. Cortical current density reconstruction of interictal epileptiform activity in temporal lobe epilepsy. *Clinical Neurophysiology*, 112(9):1761 – 1772, 2001.

[48] Akio Ikeda and Yushi Inoue. *Event-related Potentials in Patients with Epilepsy: from Current State to: Future Prospects*, volume 5. John Libbey Eurotext, 2008.

[49] Arne Jensen and Anders la Cour-Harbo. *Ripples in mathematics: the discrete wavelet transform.* springer, 2001.

[50] C. Juhasz and H. T. Chugani. Imaging the epileptic brain with positron emission tomography. *Neuroimaging Clin. N. Am.*, 13(4):705–716, Nov 2003.

[51] Robert C Knowlton, Rotem a Elgavish, Al Bartolucci, Buddhiwardhan Ojha, Nita Limdi, Jeffrey Blount, Jorge G Burneo, Lawrence Ver Hoef, Lebron Paige, Edward Faught, Pongkiat Kankirawatana, Kristen Riley, and Ruben Kuzniecky. Functional imaging: II. Prediction of epilepsy surgery outcome. *Annals of neurology*, 64(1):35–41, July 2008.

[52] Katsuhiro Kobayashi, Harumi Yoshinaga, Yoko Ohtsuka, and Jean Gotman. Dipole modeling of epileptic spikes can be accurate or misleading. *Epilepsia*, 46(3):397–408, 2005.

[53] Laurent Koessler, Christian Benar, Louis Maillard, Jean-Michel Badier, Jean Pierre Vignal, Fabrice Bartolomei, Patrick Chauvel, and Martine Gavaret. Source localization of ictal epileptic activity investigated by high resolution EEG and validated by SEEG. *NeuroImage*, 51(2):642–53, June 2010.

[54] Jan Kybic, Maureen Clerc, Toufic Abboud, Olivier Faugeras, Renaud Keriven, and Tho Papadopoulo. A common formalism for the integral formulations of the forward EEG problem. *IEEE Transactions on Medical Imaging*, 24(1):12–28, January 2005. PMID: 15638183.

[55] Jan Kybic, Maureen Clerc, Olivier Faugeras, Renaud Keriven, and Theo Papadopoulos. Generalized Head Models for MEG / EEG : BEM beyond Nested Volumes. *Physics in Medicine and Biology*, 2006.

[56] Göran Lantz, Laurent Spinelli, Margitta Seeck, Rolando Grave de Peralta Menendez, Cyrille C Sottas, and Christoph M Michel. Propagation of interictal epileptiform activity can lead to erroneous source localizations: a 128-channel EEG mapping study. *Journal of clinical neurophysiology : official publication of the American Electroencephalographic Society*, 20(5):311–9, 2003.

[57] Ervig Lapalme, Jean-Marc Lina, and Jérémie Mattout. Data-driven parceling and entropic inference in MEG. *NeuroImage*, 30(1):160–71, March 2006.

[58] J Lina, R Chowdhury, E Lemay, E Kobayashi, and C Grova. Wavelet-based localization of oscillatory sources from magnetoencephalography data. *IEEE transactions on bio-medical engineering*, (c):1–15, March 2012.

[59] AK Liu, AM Dale, and JW Belliveau. Monte Carlo simulation studies of EEG and MEG localization accuracy. *Human brain mapping*, 62:47–62, 2002.

[60] A. Machado, J.M. Lina, J. Tremblay, M. Lassonde, D.K. Nguyen, F. Lesage, and C. Grova. Detection of hemodynamic responses to epileptic activity using simultaneous electro-encephalography (EEG)/near infra red spectroscopy (NIRS) acquisitions. *NeuroImage*, 56(1):114 – 125, 2011.

[61] J. Mattout, M. Plgrini-Issac, L. Garnero, and H. Benali. Multivariate source prelocalization (MSP): Use of functionally informed basis functions for better conditioning the MEG inverse problem. *NeuroImage*, 26(2):356 – 373, 2005.

[62] William Menke. *Geophysical data analysis: discrete inverse theory*, volume 45. Access Online via Elsevier, 1989.

[63] C E Metz. ROC methodology in radiologic imaging. *Investigative Radiology*, 21(9):720–733, 1986.

[64] A. Molins, S. M. Stufflebeam, E. N. Brown, and M. S. Hamalainen. Quantification of the benefit from integrating MEG and EEG data in minimum l2-norm estimation. *Neuroimage*, 42(3):1069–1077, Sep 2008.

[65] J. C. Mosher, R. M. Leahy, and P. S. Lewis. EEG and MEG: forward solutions for inverse methods. *IEEE Trans Biomed Eng*, 46(3):245–259, Mar 1999.

[66] J.C. Mosher, P.S. Lewis, and R.M. Leahy. Multiple dipole modeling and localization from spatio-temporal MEG data. *Biomedical Engineering, IEEE Transactions on*, 39(6):541 –557, june 1992.

[67] Shingo Murakami and Yoshio Okada. Contributions of principal neocortical neurons to magnetoencephalography and electroencephalography signals. *The Journal of physiology*, 575(Pt 3):925–36, September 2006.

[68] Thomas E Nichols and Andrew P Holmes. Nonparametric permutation tests for functional neuroimaging: a primer with examples. *Human brain mapping*, 15(1):1–25, January 2002.

[69] E. Niedermeyer. *Abnormal EEG patterns: epileptic and paroxysmal*, chapter 13, pages 255–280. Niedermayer, E. and Lopes da Silva, F, electroencephalography, basic principles, clinical applications and related fields edition, 1993.

[70] Soheyl Noachtar and Jan Rémi. The role of EEG in epilepsy: A critical review. *Epilepsy & Behavior*, 15(1):22 – 33, 2009. Management of Epilepsy: Hope and Hurdles - Critical Reviews and Clinical Guidance.

[71] S. Ogawa, T. M. Lee, A. R. Kay, and D. W. Tank. Brain magnetic resonance imaging with contrast dependent on blood oxygenation. *Proc. Natl. Acad. Sci. U.S.A.*, 87(24):9868–9872, Dec 1990.

[72] Makoto Oishi, Hiroshi Otsubo, Shigeki Kameyama, Nobuhito Morota, Hiroshi Masuda, Masaomi Kitayama, and Ryuichi Tanaka. Epileptic spikes:

magnetoencephalography versus simultaneous electrocorticography. *Epilepsia*, 43(11):1390–5, November 2002.

[73] Nobuyuki Otsu. A threshold selection method from gray-level histograms. *Systems, Man and Cybernetics, IEEE Transactions on*, 9(1):62 –66, jan. 1979.

[74] W Ou, M Hämäläinen, and P Golland. A distributed spatio-temporal EEG/MEG inverse solver. *Med Image Comput Comput Assist Interv*, 2008.

[75] Dimitrios Pantazis, Thomas E Nichols, Sylvain Baillet, and Richard M Leahy. A comparison of random field theory and permutation methods for the statistical analysis of MEG data. *NeuroImage*, 25(2):383–94, April 2005.

[76] RD Pascual-Marqui et al. Standardized low-resolution brain electromagnetic tomography (sloreta): technical details. *Methods Find Exp Clin Pharmacol*, 24(Suppl D):5–12, 2002.

[77] Roberto D Pascual-Marqui, Christoph M Michel, and Dietrich Lehmann. Low resolution electromagnetic tomography: a new method for localizing electrical activity in the brain. *International Journal of psychophysiology*, 18(1):49–65, 1994.

[78] J. Sarvas. Basic mathematical and electromagnetic concepts of the biomagnetic inverse problem. *Phys Med Biol*, 32(1):11–22, Jan 1987.

[79] M. Scherg. Fundamentals of dipole source potential analysis. 1990.

[80] Kensuke Sekihara, Maneesh Sahani, and Srikantan S Nagarajan. Bootstrap-based statistical thresholding for MEG source reconstruction images. *Conference proceedings : ... Annual International Conference of the IEEE Engineering in Medicine and Biology Society. IEEE Engineering in Medicine and Biology Society. Conference*, 2:1018–21, January 2004.

[81] F. Sharbrough, G. E. Chatrian, R.P. Lesser, H. Luders, M. Nuwer, and TW. Picton. American electroencephalographic society guidelines for standard electrode position nomenclature. *Journal of Clinical Neurophysiology*, 1991.

[82] Charles Stangor. *Introduction to psychology.*

[83] M. Strandberg, E. M. Larsson, S. Backman, and K. Kallen. Pre-surgical epilepsy evaluation using 3T MRI. Do surface coils provide additional information? *Epileptic Disord*, 10(2):83–92, Jun 2008.

[84] W. W. Sutherling, A. N. Mamelak, D. Thyerlei, T. Maleeva, Y. Minazad, L. Philpott, and N. Lopez. Influence of magnetic source imaging for planning intracranial EEG in epilepsy. *Neurology*, 71(13):990–996, Sep 2008.

[85] Naoaki Tanaka, Matti S Hämäläinen, Seppo P Ahlfors, Hesheng Liu, Joseph R Madsen, Blaise F Bourgeois, Jong Woo Lee, Barbara A Dworetzky, John W Belliveau, and Steven M Stufflebeam. Propagation of epileptic spikes reconstructed from spatiotemporal magnetoencephalographic and electroencephalographic source analysis. *NeuroImage*, 50(1):217–22, March 2010.

[86] James X Tao, Maria Baldwin, Susan Hawes-Ebersole, and John S Ebersole. Cortical substrates of scalp eeg epileptiform discharges. *Journal of clinical neurophysiology*, 24(2):96–100, 2007.

[87] Nelson J. Trujillo-Barreto, Eduardo Aubert-Vzquez, and William D. Penny. Bayesian M/EEG source reconstruction with spatio-temporal priors. *NeuroImage*, 39(1):318 – 335, 2008.

[88] W. Van Paesschen, P. Dupont, S. Sunaert, K. Goffin, and K. Van Laere. The use of SPECT and PET in routine clinical practice in epilepsy. *Curr. Opin. Neurol.*, 20(2):194–202, Apr 2007.

[89] B.D. Van Veen, W. Van Drongelen, M. Yuchtman, and A. Suzuki. Localization of brain electrical activity via linearly constrained minimum variance spatial filtering. *Biomedical Engineering, IEEE Transactions on*, 44(9):867 –880, sept. 1997.

[90] Thaddeus S. Walczak, Prasanna Jayakar, and Eli M. Mizrahi. *Epilepsy: a comprehensive textbook*, chapter Interictal ElectroEncephaloGraphy. Volume 1 of [27], 2008.

[91] S Wiebe, D R Bellhouse, C Fallahay, and M Eliasziw. Burden of epilepsy: the Ontario Health Survey. *The Canadian journal of neurological sciences. Le journal canadien des sciences neurologiques*, 26(4):263–70, November 1999.

[92] CH Wolters. The finite element method in eeg/meg source analysis. *SIAM News*, 40(2), 2007.

[93] Max Woodbury. Inverting Modified Matrices SE - Statistical Research Group Memorandum Reports. Number 42. Princeton University, Princeton, NJ, 1950.

[94] K J Worsley, S Marrett, P Neelin, a C Vandal, K J Friston, and a C Evans. A unified statistical approach for determining significant signals in images of cerebral activation. *Human brain mapping*, 4(1):58–73, January 1996.

[95] Yang Xu, Gustavo P Sudre, Wei Wang, Douglas J Weber, and Robert E Kass. Characterizing global statistical significance of spatiotemporal hot spots in magnetoencephalography/ electroencephalography source space via excursion algorithms. *Statistics in medicine*, 30(23):2854–66, October 2011.

[96] JE Zimmerman, Paul Thiene, and JT Harding. Design and operation of stable rf-biased superconducting point-contact quantum devices, and a note on the properties of perfectly clean metal contacts. *Journal of Applied Physics*, 41(4):1572–1580, 1970.